Origin of δ13C minimum events in thermocline and intermediate waters of the western South Atlantic

R.A. Nascimento, T.P. Santos, I.M. Venancio, C.M. Chiessi, J.M. Ballalai, H. Kuhnert, A. Govin, R.C. Portilho-Ramos, D. Lessa, B.B. Dias, et al.

Origin of $\delta^{13}C$ minimum events in thermocline and intermediate waters of the western South Atlantic

Nascimento, R. A[1*]; Santos, T. P.[1]; Venancio, I. M.[1,2]; Chiessi, C. M.[3]; Ballalai, J. M.[1]; Kuhnert, H.[4]; Govin, A.[5]; Portilho-Ramos, R. C.[4]; Lessa, D.[1]; Dias, B. B.[1,3]; Pinho, T. M. L.[6]; Crivellari, S.[3]; Mulitza, S.[4]; Albuquerque, A. L. S.[1]

[1] Programa de Geociências (Geoquímica), Universidade Federal Fluminense, Niterói, Brazil

[2] Center for Weather Forecasting and Climate Studies (CPTEC), National Institute for Space Research (INPE), Cachoeira Paulista, Brazil

[3] School of Arts, Sciences and Humanities, University of São Paulo, São Paulo, Brazil

[4] MARUM - Center for Marine Environmental Sciences, University of Bremen, Bremen, Germany

[5] Laboratoire des Sciences du Climat et de l'Environnement/Institut Pierre Simon Laplace, CEA-CNRS-UVSQ, Université Paris Saclay, Gif sur Yvette, France

[6] Institute of Geosciences, University of São Paulo, São Paulo, Brazil

*Corresponding author

e-mail address: rodrigoan@id.uff.br

Keywords: stable carbon isotopes, $\delta^{13}C$ minimum events, glacial terminations, western South Atlantic

Abstract

Stable carbon isotopic ($\delta^{13}C$) minimum events have been widely described in marine archives recording the properties of thermocline and intermediate waters during glacial terminations. However, the mechanisms associated with these events remain ambiguous. Here we present three high temporal resolution deep-dwelling planktonic foraminifera $\delta^{13}C$ records from the main thermocline and one benthic $\delta^{13}C$ record from the modern core of Antarctic Intermediate Water (AAIW). Our sediment cores are distributed along the western South Atlantic from the equator to the subtropics, with the longest record spanning the last ~300 kyr. The results show that $\delta^{13}C$ minimum events were pervasive features of the last three glacial terminations and Marine Isotope Stage 4/3 transition in the western South Atlantic. Two distinct mechanisms were responsible for the $\delta^{13}C$ minima at the thermocline and intermediate depths of the Atlantic, respectively. We suggest that the $\delta^{13}C$ minimum events at the thermocline were mostly driven by the thermodynamic ocean-atmosphere isotopic equilibration, which is supported by calculated $\delta^{13}C$ of dissolved inorganic carbon in the subtropical western

South Atlantic as well as by previously published model simulations. On the other hand, intermediate depths $\delta^{13}C$ minimum events in the tropics were likely caused by the slowdown of the Atlantic meridional overturning circulation and the associated accumulation of isotopically light carbon at mid and intermediate depths of the Atlantic Ocean.

1. Introduction

Upwelling in the Southern Ocean (SO) connects the deep ocean with the atmosphere, by drawing deep waters to the SO surface (Marshall and Speer, 2012). The deep ocean is hypothesized to have been the main sink of atmospheric CO_2 during glacial periods, as evidenced by the accumulation of ^{13}C-depleted remineralized carbon in poorly ventilated deep waters below ~2500 m water depth (Hodell et al., 2003; Howe et al., 2016a; Curry and Oppo, 2005). Across glacial terminations, the breakup of deep-ocean stratification (e.g., Du et al., 2018; Basak et al., 2018) and the intensification of upwelling in the SO have been linked to the advection of nutrient-rich ^{13}C-depleted waters from the deep ocean to the SO surface (Anderson et al., 2009; Toggweiler et al., 2006). This was followed by atmospheric CO_2 increase and stable carbon isotopic ($\delta^{13}C$) minimum events at thermocline and intermediate depths of the oceans (between 100 and 1200 m water depth) (e.g., Martínez-Botí et al., 2015; Ziegler et al., 2013; Schmitt et al., 2012; Spero and Lea, 2002). A widely held hypothesis behind these $\delta^{13}C$ minimum events is the northward transport of ^{13}C-depleted carbon from the SO surface towards the equatorial regions by Subantarctic Mode Water (SAMW) and Antarctic Intermediate Water (AAIW) (Spero and Lea, 2002). This mechanism is named the “oceanic tunnel” (Liu and Yang, 2003). In the Atlantic Ocean, the “oceanic tunnel” hypothesis is supported by the occurrence of $\delta^{13}C$ minimum events in thermocline and intermediate depth records from the tropical region (e.g., Poggemann et al., 2017; Mulitza et al., 1998). However, $\delta^{13}C$ minimum events have also been observed in regions far from the influence of SAMW and AAIW as, for example, in the North Atlantic (e.g., Lynch-Stieglitz et al., 2019; Rickaby and Elderfield, 2005). Additionally, intermediate depth records in subtropical latitudes of the Southern Hemisphere

lack evidence of $\delta^{13}C$ minimum events. For instance, depth transects along the southern Brazilian margin (~27°S) do not support the presence of a ^{13}C-depleted northward flowing AAIW during Termination I (Lund et al., 2015; Tessin and Lund, 2013; Oppo and Horowitz, 2000). Accordingly, other mechanisms have been raised to explain the occurrence of the $\delta^{13}C$ minimum events.

The outgassing of ^{13}C-depleted CO_2 to the atmosphere during glacial terminations resulted in an atmospheric ^{13}C depletion similar to that observed in the upper ocean (Eggleston et al., 2016; Schmitt et al., 2012). Consequently, it has been suggested that temperature-mediated ocean-atmosphere isotopic equilibration could explain the widespread occurrence of $\delta^{13}C$ minimum events in the ocean (Shao et al., 2021; Lynch-Stieglitz et al., 2019; Ninnemann and Charles, 1997). According to this mechanism, the ocean-atmosphere isotopic equilibration would globally imprint the $\delta^{13}C$ minimum signal in the upper ocean and possibly at intermediate and mid-depth waters at the formation region of these water masses.

Alternatively, $\delta^{13}C$ minima at intermediate depths of the tropical Atlantic may also have been caused by changes in the dynamics of the Atlantic meridional overturning circulation (AMOC) during glacial terminations, as indicated by model simulations (Menviel et al., 2018; Schmittner and Lund, 2015). Some studies have suggested that the reduced ventilation rate of North Atlantic Deep Water (NADW), which forms the lower limb of the AMOC, caused the observed ^{13}C depletion in the mid-depth of the Atlantic Ocean during the last glacial termination (Campos et al., 2020; Lacerra et al., 2017; Schmittner and Lund, 2015; Lund et al., 2015). Accordingly, this northern sourced ^{13}C-depletion may have expanded upwards into intermediate depths (~1000 m water depth) in the tropical Atlantic (Voigt et al., 2017; Freeman et al., 2015). Ultimately, this could imply a northern origin for the $\delta^{13}C$ minimum signal at intermediate depths of tropical regions.

Here we investigate the occurrence and origin of the $\delta^{13}C$ minimum events at the thermocline and intermediate depths of the western South Atlantic during the last three glacial terminations. We present three new high-resolution planktonic foraminiferal $\delta^{13}C$ records from South Atlantic Central Water (SACW) and one record from AAIW extending from the equator

to the southern subtropical latitudes along the Brazilian margin (Fig. 1). Our results point to two distinct and independent mechanisms governing the $\delta^{13}C$ minimum events at the thermocline and intermediate depths. At the thermocline, ^{13}C-depletions were mostly driven by the ocean-atmosphere isotopic equilibration, while AMOC slowdown was mostly responsible for the ^{13}C-depletion at intermediate depths.

2. Regional settings

The South Atlantic upper-ocean circulation is dominated by the South Atlantic Subtropical Gyre (SASG) (Fig. 1a). The northernmost and the southernmost limits of the SASG are marked by the South Equatorial Current (SEC) and the South Atlantic Current (SAC), respectively. The westward-flowing SEC gives rise to the southward-flowing Brazil Current (BC) and the northward-flowing North Brazil Undercurrent and North Brazil Current. At about 38°S, the BC converges with the northward-flowing Malvinas Current, giving rise to the SAC that flows eastwards. Ultimately, the SAC feeds the SEC, which returns to the Brazilian coast, closing the gyre (Peterson and Stramma, 1991).

The water masses filling thermocline and intermediate depths of the western South Atlantic are SACW and AAIW (Fig. 1b), together named Southern Ocean intermediate waters (SOIWs). The SACW occupies the South Atlantic thermocline between approximately 100 to 500 m water depth. This water mass shows wide temperature (5°C to 20°C) and salinity (34.3 to 36) ranges (Stramma and England, 1999). A portion of SACW is formed in the Brazil-Malvinas Confluence zone (BMC) region at the subtropical convergence (Sprintall and Tomczak, 1993). During austral winter, the thick and homogeneous SAMW subducts in the subtropical convergence, producing SACW, which moves eastward within the SAC and recirculates in the SASG (Stramma and England, 1999). In the southeast Atlantic, another portion of SACW is formed by the injection of Indian Ocean waters into the South Atlantic in the Agulhas Current retroflection region (Poole and Tomczak, 1999; Sprintall and Tomczak, 1993; Gordon, 1986). Below the SACW, AAIW is marked by minimum salinity between approximately 500 to 1500 m water depth (Fig. 1b). The temperature and salinity of the AAIW range between 2°C to 6°C

and 33.8 to 34.8, respectively (Emery and Meincke, 1986). AAIW is mainly formed by overturning convection in the extreme east of the South Pacific Ocean, enters the southwestern Atlantic through the Drake Passage, and is carried northward in the Malvinas Current (England et al. 1993). Northeast of the Drake Passage and at the BMC, mixing and eddy formation inject AAIW into the South Atlantic subsurface (Stramma and England 1999; Talley, 1996). Additionally, substantial amounts of AAIW enter the Atlantic from the Indian Ocean through Agulhas Current leakage around the southern tip of Africa (Stramma and England, 1999).

Below AAIW, the NADW fills the mid-depth of the Atlantic Ocean between ~1500 and 4000 m water depth. In the modern ocean, the core of NADW is centered at 2400 m water depth (Fig. 1b). However, during the Last Glacial Maximum (LGM), NADW is estimated to have shallowed to ~1800 m water depth (Gebbie, 2014). This water mass is formed in high latitudes of the North Atlantic through buoyancy loss and convection of dense upper ocean waters in the Labrador and Nordic Seas. NADW is featured by a salinity maximum (above 34.9) at mid-depth of the Atlantic Ocean (Fig. 1b) and a temperature ranging between 2 and 4°C (Tomczak and Godfrey, 1994).

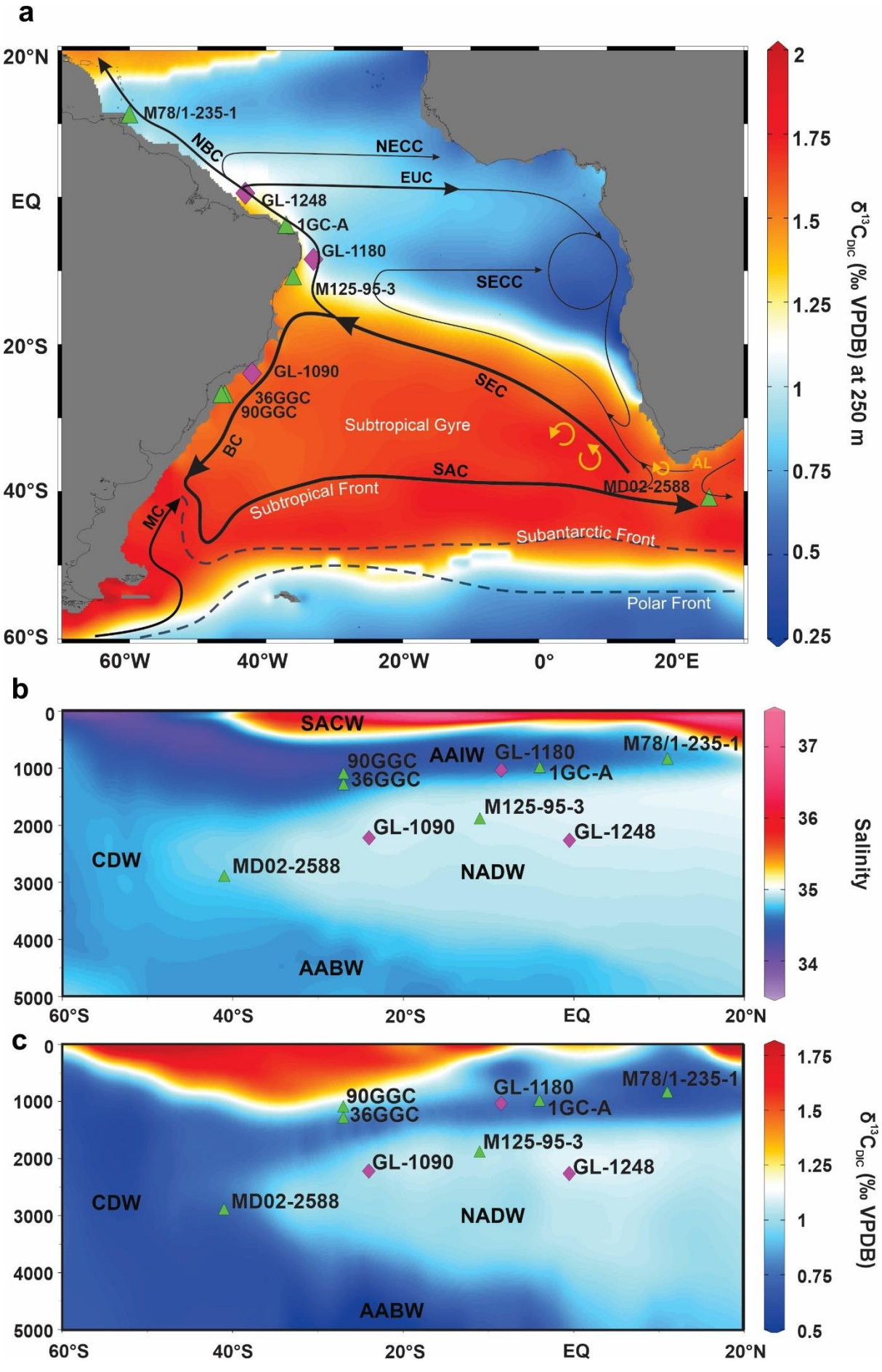
a
20°N
EQ
20°S
40°S
60°S
60°W
40°W
20°W
0°
20°E
M78/1-235-1
NBC
NECC
EUC
GL-1248
1GC-A
GL-1180
M125-95-3
SECC
GL-1090
36GGC
90GGC
SEC
Subtropical Gyre
BC
SAC
AL
MD02-2588
MC
Subtropical Front
Subantarctic Front
Polar Front
2
1.75
1.5
1.25
1
0.75
0.5
0.25
δ13CDIC (‰ VPDB) at 250 m
b
SACW
AAIW
90GGC
36GGC
GL-1180
1GC-A
M78/1-235-1
M125-95-3
GL-1090
GL-1248
CDW
MD02-2588
NADW
AABW
0
1000
2000
3000
4000
5000
60°S
40°S
20°S
EQ
20°N
37
36
35
34
Salinity
c
90GGC
36GGC
GL-1180
1GC-A
M78/1-235-1
M125-95-3
GL-1090
GL-1248
CDW
MD02-2588
NADW
AABW
1.75
1.5
1.25
1
0.75
0.5
δ13CDIC (‰ VPDB)

Figure 1. Location of the sediment cores analyzed in this study (pink diamonds) and other sediment cores discussed within the text (green triangles). a) Atlantic Ocean pre-industrial stable carbon isotopic composition of the dissolved inorganic carbon ($\delta^{13}C_{DIC}$) at 250 m water depth (Eide et al. 2017). Black arrows schematically represent the large-scale geostrophic currents between 100- and 500 m water depth. The dashed line depicts the Subantarctic and Polar Fronts (Orsi et al., 1995). Orange arrows depict the Agulhas leakage rings (adapted from Stramma and England, 1999). BC: Brazil Current; EUC: Equatorial Under Current; MC: Malvinas Current; NBC: North Brazil Current; NECC: North Equatorial Countercurrent; SAC: South Atlantic Current; SEC: South Equatorial Current; SECC: South Equatorial Countercurrent. b) Western Atlantic Ocean meridional section of salinity (Zweng et al., 2018); c) Western Atlantic Ocean meridional section of the pre-industrial $\delta^{13}C_{DIC}$ (Eide et al., 2017). In both sections, AABW: Antarctic Bottom Water; AAIW: Antarctic Intermediate Water; CDW: Circumpolar Deep Water; NADW: North Atlantic Deep Water; SACW: South Atlantic Central Water. In all panels, purple diamonds indicate sediment cores GL-1248, GL-1180, and GL-1090 (this study), while green triangles indicate the sediment cores M125-95-3 (Campos et al., 2020), GS07-150-17/1GC-A (1GC-A in the figure) (Freeman et al., 2015), M78/1-235-1 (Poggemann et al., 2017), KNR159-5-90GGC (Lund et al., 2015), KNR-159-5-36GGC (Tessin and Lund, 2013), and MD02-2588 (Ziegler et al., 2013). The figure was partially generated using the software Ocean Data View (Schlitzer, 2017).

The global deep ocean circulation can be separated in the upper and lower cells (Toggweiler et al., 2006; Talley, 2013). Over the SO, the westerlies force northward Ekman transport, which is compensated by the upwelling of Circumpolar Deep Water (CDW) in the Antarctic Zone (Marshall and Speer, 2012; Toggweiler and Samuels, 1995). In the upper cell, which is more limited to the Atlantic Ocean, SOIWs composed by the lightest portion of CDW will feed the formation of the NADW in the North Atlantic. In the lower cell, the densest portion of CDW moves towards the Antarctic continental shelf to form Antarctic Bottom Water (AABW), which flows northward, occupying the ocean abyss below approximately 4000 m

156 water depth (Pellichero et al., 2018; Abernathey et al., 2016; Talley, 2013). In the modern
157 ocean, there is an interplay between these two cells (Talley, 2013).

158 The spatial distribution of South Atlantic stable carbon isotopic composition of dis-
159 solved inorganic carbon ($\delta^{13}C_{DIC}$) at 250 m water depth (Fig 1a) reveals the oligotrophic and
160 high $\delta^{13}C_{DIC}$ SASG (warm tones in Fig. 1a), while in the equatorial and eastern tropical Atlantic
161 (Guinea and Angola domes), reduced ventilation and high productivity and remineralization of
162 organic carbon result in $^{13}C_{DIC}$-depleted subsurface waters (cold tones in Fig. 1a). The merid-
163 ional $\delta^{13}C_{DIC}$ section from the western tropical and South Atlantic Ocean (Fig 1c) exhibits the
164 pattern of ^{13}C-depletion at thermocline and intermediate depths in the tropics. Oppo et al.
165 (2018) show that remineralization is responsible for up to 1‰ of $\delta^{13}C_{DIC}$ depletion at thermo-
166 cline and intermediate depth in the western tropical Atlantic. Approximately, 60% of this re-
167 mineralization occurs near the formation site of AAIW, while the rest occurs as AAIW advects
168 northward. The vertical $\delta^{13}C_{DIC}$ profile at about 20°S is marked by a decrease from the oligo-
169 trophic SASG (~1.5 ‰) downward through the SACW and AAIW until reaching the minimum
170 of ~0.7 ‰ at 1300 m water depth, reflecting the influence of Upper Circumpolar Deep Water.
171 Below that, $\delta^{13}C_{DIC}$ increases again due to the $^{13}C_{DIC}$-enriched NADW (~1 ‰) that flows south-
172 ward between 1500 and 4000 m water depth. Finally, in the South Atlantic abyss, the $^{13}C_{DIC}$-
173 depleted AABW (~0.5 ‰) flows northward, underlying NADW.

174 **3. Methods**

175 **3.1. Sediment cores**

176 In this study, we present new data from sediment cores GL-1248 (0°55'20" S,
177 43°24'10" W, 2264 m water depth, 19.29 m long) from the Brazilian equatorial margin, GL-
178 1180 (8°27'18" S, 33°32'53" W, 1037 m water depth, 17.32 m long) from the Brazilian tropical
179 margin and GL-1090 (24°55'12'' S, 42°30'36'' W, 2225 m water depth, 19.14 m long) from the
180 Brazilian subtropical margin (Fig 1). All sediment cores were provided by the Brazilian oil com-
181 pany Petrobras. A visual analysis of the core sections does not indicate any sedimentation
182 disturbance, except for a hiatus between 2.18 and 1.70 m in core GL-1248 (Venancio et al.,

2018). The three cores were sampled at 2 cm resolution with sample volume of approximately 10 cm^3. Samples were wet-sieved to retain the fraction larger than 63 μm. The retained material was dried at 50°C for 24 hours and stored in acrylic containers. Foraminifera shells were handpicked using a binocular microscope.

3.2. Age model

We used the published age model of core GL-1248 (Venancio et al., 2018), based on twelve calibrated radiocarbon ages and the visual alignment of its Ti/Ca ratio to the Greenland stable oxygen isotope ($\delta^{18}O$) record (NGRIP members, 2004), using the extended Greenland Ice Core Chronology (GICC05modelext) (Wolff et al., 2010). This alignment assumes that Ti/Ca peaks resulting from increased precipitation in the northeast Brazilian region correspond to North Atlantic cold events (e.g., Zhang et al., 2017). GL-1248 was sampled relatively close to the Parnaíba River mouth and was significantly influenced by terrigenous input during periods of low sea levels and high precipitation periods in northeastern Brazil (Venancio et al., 2018). The age model was built using the software Clam 2.2 (Blaauw, 2010), with GL-1248 spanning the last 124 ka, and was described in detail by Venancio et al. (2018).

The age model of core GL-1180 was published by Nascimento et al. (2021) and is based on six calibrated radiocarbon ages (Supporting Information, Table S1) and the alignment of the benthic $\delta^{18}O$ record of *Cibicides* spp. with the global $\delta^{18}O$ stack LR04 (Lisiecki and Raymo, 2005) (Table S2 and Fig. S1). The benthic $\delta^{18}O$ tie point uncertainties were calculated following the recommendations by Govin et al. (2015). The calculation used the uncertainties of the reference stack and of the alignment procedure, as well as the resolutions of the reference stack and of the target record. Radiocarbon ages were calibrated using the IntCal13 calibration curve (Reimer et al., 2013), with a reservoir effect of 400 ± 200 without any additional local reservoir effect. The age model (Fig. S1) was built using the software Bacon v 2.3 (Blaauw and Christen, 2011); it shows that sediment core GL-1180 spans the last 300 kyr. More details about the age model can be found in Nascimento et al. (2021).

For core GL-1090, we use the age model previously published by Santos et al. (2017) and improved by Ballalai et al. (2019) and Santos et al. (2020). It is based on ten calibrated radiocarbon ages and the alignment of its benthic $\delta^{18}O$ record of (*Cibicides wuellerstorfi*) with the benthic $\delta^{18}O$ records from the reference curves LR04 (Lisiecki and Raymo, 2005) and MD95-2042 (Govin et al., 2014). The age model was built using the software Bacon v 2.3 (Blaauw and Christen, 2011), with GL-1090 covering the last 182 kyr.

3.3. Foraminifera stable carbon isotopes ($\delta^{13}C$) analysis

Our $\delta^{13}C_{DIC}$ reconstruction of SACW is based on the $\delta^{13}C$ data from thermocline-dwelling foraminifera *Neogloboquadrina dutertrei* (GL-1248), *Globorotalia truncatulinoides* (dextral) (GL-1180), and *Globorotalia inflata* (GL-1090). The apparent calcification depth (ACD) of *N. dutertrei* was estimated to be 150 m in the region of core GL-1248 (Venancio et al. 2018), in line with previous estimates in the tropical Atlantic (Cléroux et al., 2013; Farmer et al., 2007; Steph et al., 2009). *G. truncatulinoides* presents a wide vertical migration range during its life cycle but primarily calcifies at the main thermocline (Steph et al., 2009; Regenberg et al., 2009; Cléroux et al., 2007; LeGrande et al., 2004), which is consistent with an ACD of ~250 m in the region of core GL-1180 (Nascimento et al., 2021). In the western South Atlantic, the *G. inflata* ACD stably ranges from 350 to 400 m water depth (Groeneveld and Chiessi, 2011).

Between 5 and 10 shells of *N. dutertrei* (350-415 μm), *G. truncatulinoides* (dextral; 300-425 μm), and *G. inflata* (250-300 μm) were handpicked from samples of cores GL-1248, GL-1180, and GL-1090, respectively. The sampling resolution varied between 2 and 4 cm downcore.

Our reconstruction of seawater $\delta^{13}C$ for intermediate depth is based on $\delta^{13}C$ from benthic foraminifera *Cibicides* spp. from core GL-1180 (1037 m water-depth). To do so, between 5 and 10 shells of *Cibicides* spp. (300-350 μm), composed by *Cibicides pachyderma, Cibicides refulgens,* and *Cibicides kullenbegi* (Supporting Information, Text S1), were handpicked at 4 cm resolution.

Analyses of planktonic foraminifera from the cores GL-1248 and GL-1090, and benthic foraminifera from GL-1180 were carried out in the Center for Marine Environmental Sciences (MARUM), University of Bremen, Germany, using a Finnigan MAT 251 isotope ratio mass spectrometer (IRMS) equipped with an automated carbonate preparation device (Kiel I). Data were calibrated against the in-house standard (Solnhofen limestone), and the standard deviation of the in-house standard over the measurement period was 0.03 ‰. Analyses of planktonic foraminifera from core GL-1180 were performed in the Paleoceanography and Paleoclimatology Laboratory, University of São Paulo, Brazil, using a Thermo™ Scientific MAT 253 IRMS coupled to a Thermo™ Kiel IV automated carbonate preparation device (Kiel IV) (Crivellari et al., 2021). Data were calibrated against the NBS 19 standard. The standard deviation of NBS 19 over the measurement period was 0.02 ‰. All data are presented in parts per thousand (‰) relative to the Vienna Pee Dee belemnite (VPDB).

4. Results

The $\delta^{13}C$ of *N. dutertrei* (GL-1248) ranges between 1.11 and 2.29 ‰ (mean 1.70 ± 0.17 ‰), while the $\delta^{13}C$ range is from 0.23 to 1.93 ‰ (mean 1.21 ± 0.21 ‰) for *G. truncatulinoides* (GL-1180), and between 0.06 to 1.47 ‰ (mean 0.80 ± 0.19 ‰) for *G. inflata* (GL-1090) (Fig. 2). Planktonic $\delta^{13}C$ records from all studied cores present a similar pattern with remarkable negative excursions during glacial terminations that only recover after the onset of the following interglacial period (Fig. 2). The records show little difference between glacial and interglacial $\delta^{13}C$ values. A prominent negative excursion is also observed during the transition between Marine Isotope Stage (MIS) 4 and MIS 3. In general, the benthic $\delta^{13}C$ record from core GL-1180 is similar to the thermocline $\delta^{13}C$ records (Fig 2a). The average benthic $\delta^{13}C$ is 0.64 ± 0.17 ‰, and the values range between 0.02 and 1.49 ‰, similar to *G. inflata* $\delta^{13}C$ from core GL-1090.

Termination IIIb (Fig 2d) is only recorded in sediment core GL-1180, which covers the last 300 kyr. *G. truncatulinoides* and *Cibicides* spp. $\delta^{13}C$ records show a drop of 0.4 and 0.5 ‰, respectively, relative to MIS 8. $\delta^{13}C$ minima are also observed during Termination IIIa at

263 the transition between MIS 7d and MIS 7c. A more pronounced $\delta^{13}C$ minimum occurred during
264 Termination II (Fig 2c), when *G. truncatulinoides* and *G. inflata* $\delta^{13}C$ values drop by ~0.8 and
265 ~0.4 ‰, respectively. Similarly, during Termination II, the benthic $\delta^{13}C$ record dropped by ~0.6
266 ‰ relative to MIS 6 (Fig 2c). The *N. dutertrei* $\delta^{13}C$ record spans the last 124 ka only, and its
267 oldest samples indicate that $\delta^{13}C$ is recovering from a minimum of at least 1.40 ‰ to reach
268 interglacial values of ~1.8 ‰ at 121 ka. All records show negative $\delta^{13}C$ excursions during
269 MIS4/3 transition. These excursions are equivalent to those observed during glacial termina-
270 tions. The largest drops are exhibited in *N. dutertrei* (GL-1248) and *G. inflata* (GL-1090), where
271 $\delta^{13}C$ values decrease by ~0.5 ‰. *G. truncatulinoides* and *Cibicides spp.* (GL-1180) show a
272 $\delta^{13}C$ decrease of ~0.3 ‰. During Termination I, *G. inflata* and *G. truncatulinoides* $\delta^{13}C$ drops
273 approximately 0.4 ‰ relative to MIS 2 (Fig. 2b). *G. truncatulinoides* $\delta^{13}C$ presents several
274 short-lived $\delta^{13}C$ drops within a broad negative excursion that started at ~18 ka. For *G. inflata*
275 and *G. truncatulinoides* records, fully interglacial values are reached at ~7 ka. GL-1248 pre-
276 sents a hiatus between 29 and 14 ka, but we note that $\delta^{13}C$ is low at the end of Termination I
277 and reaches interglacial values in the mid-Holocene. During Termination I, the $\delta^{13}C$ record of
278 *Cibicides* spp. shows two negative excursions of up to ~0.4 ‰ relative to the Last Glacial Max-
279 imum (LGM) (Fig 2b).

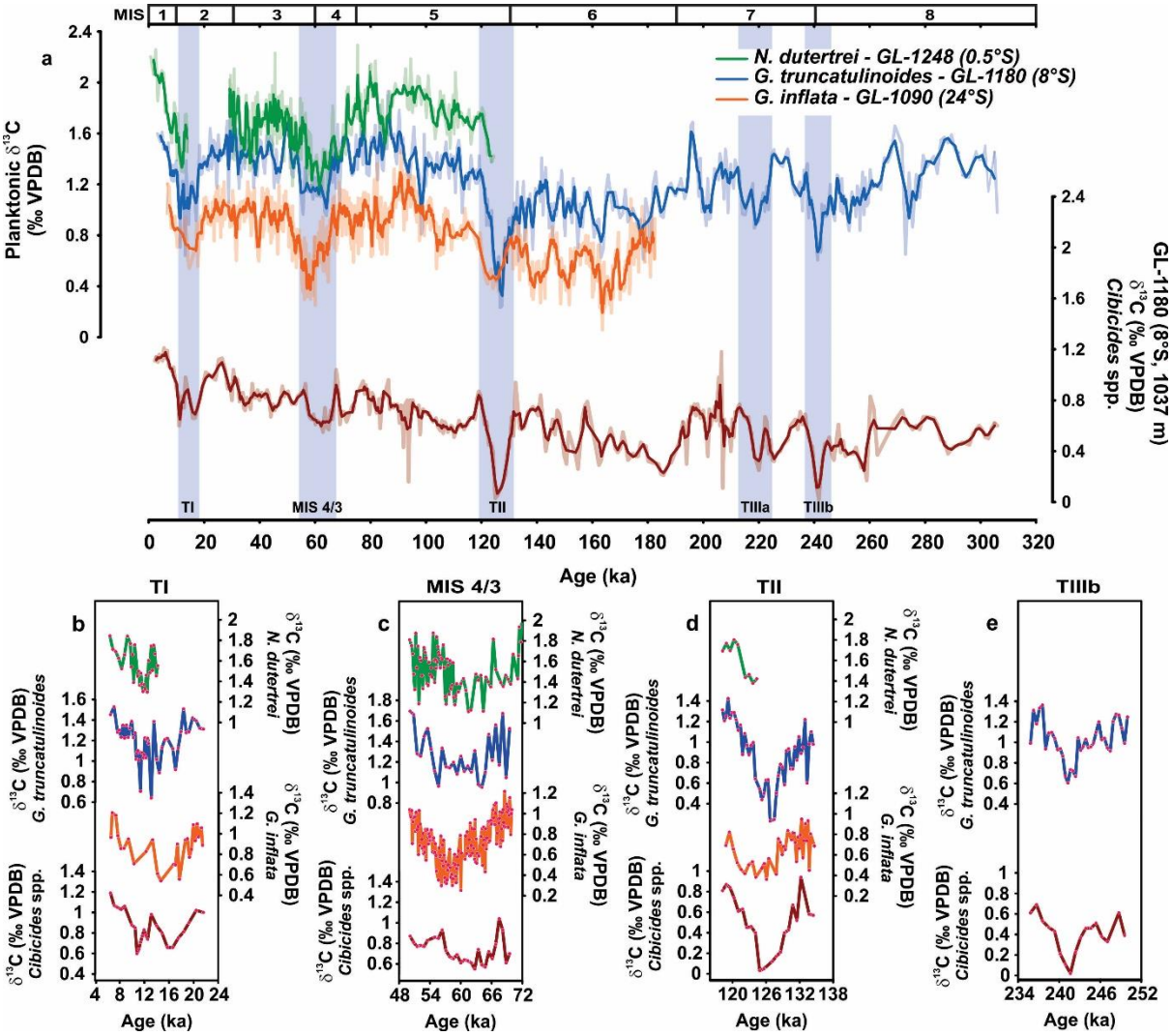

Figure 2. Carbon isotopic composition ($\delta^{13}C$) of planktonic and benthic foraminifera analyzed in this study. a) $\delta^{13}C$ of *Neogloboquadrina dutertrei* (GL-1248, green line), *Globorotalia truncatulinoides* (GL-1180, blue line), *Globorotalia inflata* (GL-1090, orange line), *Cibicides* spp. (GL-1180, dark-red line). Blue bars indicate $\delta^{13}C$ minimum events during glacial terminations and the Marine Isotope Stage (MIS) 4/3 transition. Dark colored lines depict the three points running average, while light colored lines depict the original data. Zooms of deep-dwelling and benthic $\delta^{13}C$ records for b) zoom into Termination I (TI); c) zoom into MIS4/3 transition; d) zoom into Termination II (TII); e) zoom into Termination IIIb (TIIIb) colors as in a). MIS are indicated at the top of panel a.

5. Discussion

5.1. $\delta^{13}C$ values of planktonic foraminifera

We present $\delta^{13}C$ values of three deep-dwelling planktonic foraminifera species in order to reconstruct $\delta^{13}C_{DIC}$ of thermocline waters in the western South Atlantic. Although $\delta^{13}C$ of the calcite reflects $\delta^{13}C_{DIC}$, it is not in isotopic equilibrium with seawater (Ravelo and Hillaire-Marcel, 2007). Offsets between $\delta^{13}C_{DIC}$ and $\delta^{13}C$ of calcite are related to abiotic kinetic fractionation, which causes an offset of 1.0 ± 0.2 ‰ (Romanek et al., 1992), changes in foraminifera metabolic rate (Bemis et al., 2000), seawater carbonate ion concentration (Spero et al., 1997; Wilke et al., 2006), and photosymbiosis (Spero and Deniro, 1987). The $\delta^{13}C$ from *G. truncatulinoides* and *G. inflata* is known to be dependent on shell size (Birch et al., 2013; Friedrich et al., 2012; Elderfield et al., 2002). This is likely an effect of high metabolic rates of individuals in early ontogenetic stages but analyzing shells larger than 250 µm largely avoids this effect (Birch et al., 2013; Friedrich et al., 2012). Even so, the $\delta^{13}C$ average of 11 core-tops (1.0 ‰ ± 0.2) from the western South Atlantic (Chiessi et al., 2007) shows that *G. inflata* is ~0.5 ‰ lighter than the pre-industrial $\delta^{13}C_{DIC}$ provided by Eide et al. (2017) in the same region between 350 to 400 m water depth. The same result was found in sediment trap samples from the Cape Basin (Wilke et al., 2006), suggesting that this offset is a widespread feature of this species in the South Atlantic. In the opposite direction, plankton tow samples from the equatorial Atlantic reveal that *N. dutertrei* $\delta^{13}C$ is about 0.5 ‰ higher than $\delta^{13}C_{DIC}$ (Mulitza et al., 1999). Therefore, $\delta^{13}C$ differences or similarities between foraminifera species may not only result from habitat depth but also from offsets between $\delta^{13}C_{DIC}$ and $\delta^{13}C$ of calcite. Yet, these effects mostly affect the absolute $\delta^{13}C$ values and are not expected to influence temporal changes in the downcore records, which is the central aspect discussed here.

The $\delta^{13}C$ of *G. truncatulinoides* is considered a robust proxy for nutrient content in the thermocline (Mulitza et al., 1998). *G. truncatulinoides* $\delta^{13}C$ record from GL-1180 presents a positive offset of ~0.5 ‰ relative to the same species in the Agulhas Plateau (MD02-2588, 41°S) (Ziegler et al., 2013) and in the western South Pacific (ODP1123, 41°S) (Hu et al., 2020) (Fig. 3b). Since sites MD02-2588 and ODP1123 are near central waters formation latitudes, we would presume their *G. truncatulinoides* $\delta^{13}C$ values to be higher than in the aged central waters in the tropics. The positive offset of *G. truncatulinoides* $\delta^{13}C$ in the tropics relative to

the subtropics may be related to ecological distinctions between organisms living in these regions, morphotype (dextral or sinistral), and the shell size. In the stratified tropical Atlantic, the ACD range of *G. truncatulinoides* is estimated to extend from the base of the seasonal thermocline to ~400 m water depth (Mulitza et al., 1997). In the subtropics, this species extends its life cycle from the weakly stratified ocean surface to ~800 m water depth (Mulitza et al., 1997; Ujiié et al., 2010; Hu et al., 2020). In fact, this large difference in the depth range may favor the *G. truncatulinoides* secondary calcite crust, which forms deeper in the water column (Mulitza et al., 1997), to record lower $\delta^{13}C$ values in the subtropics relative to the tropical ocean. Additionally, in contrast to Hu et al. (2020) and Ziegler et al. (2013) who analyzed the sinistral morphotype of *G. truncatulinoides*, we used the *G. truncatulinoides* dextral. Indeed, it was suggested that the dextral morphotype shows a shallower ACD and prefers a more stratified thermocline than the sinistral (Feldmeijer et al., 2014; Ujiié et al., 2010). Besides, the size fraction analyzed in our study is larger than in the aforementioned studies, reducing the effect of metabolic rate on the $\delta^{13}C$ of calcite (Birch et al., 2013; Friedrich et al., 2012). Mixing with high $\delta^{13}C$ of SASG waters (Fig. 1a, c) may also contribute to increasing the thermocline $\delta^{13}C$ in the tropics relative to the subtropics (Fig. 3b).

Despite the difference in location and species measured within GL-1090 (i.e. *G. inflata* from the SASG) to those of Ziegler et al. (2013) and Hu et al. (2020) (i.e. G*. truncatulinoides* from Agulhas Plateau and western South Pacific, respectively), the three records present similar $\delta^{13}C$ values (Fig. 3b). We ascribe this similarity to the negative ~0.5 ‰ offset of *G. inflata* $\delta^{13}C$ relative to $\delta^{13}C_{DIC}$ (Wilke et al., 2006) and to the deep ACD of *G. inflata* in the western South Atlantic (Groeneveld and Chiessi, 2011). The higher averaged $\delta^{13}C$ values observed in the *N. dutertrei* record (GL-1248) (Fig. 2a) may reflect the shallow habitat within the thermocline and the additional positive offset (0.5 ‰) relative to $\delta^{13}C_{DIC}$ observed in the equatorial Atlantic (Mulitza, 1999).

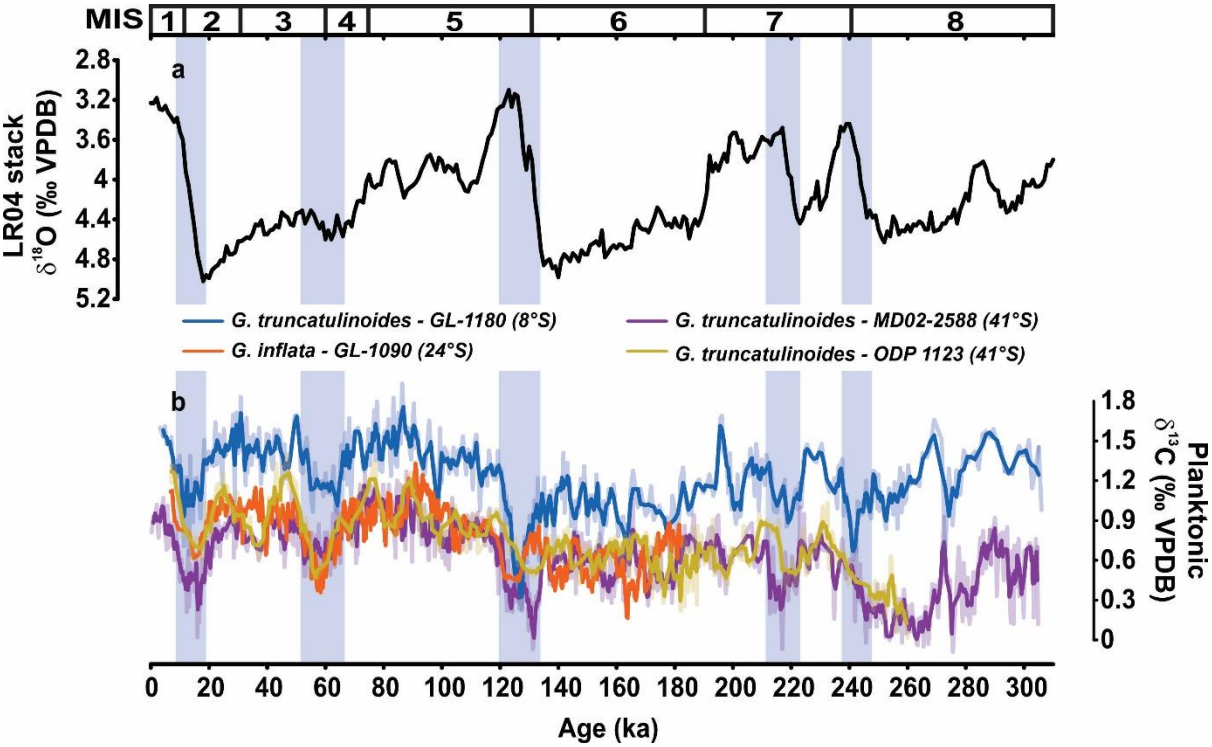

Figure 3. Stable carbon isotopic ($\delta^{13}C$) records presented in this study compared with published thermocline (see locations in Fig. 1) records. a) LR04 global oxygen stable isotopic ($\delta^{18}O$) stack (Lisiecki and Raymo, 2005). b) $\delta^{13}C$ of *Globorotalia truncatulinoides* from the western tropical South Atlantic (GL-1180, blue line), *Globorotalia inflata* from the western subtropical South Atlantic (GL-1090, orange line), *G. truncatulinoides* from the Agulhas Plateau (MD02-2588, purple line) (Ziegler et al., 2013), and *G. truncatulinoides* from the western South Pacific (ODP1123, dark yellow) (Hu et al., 2020). Dark colored lines depict the three points running average, while light colored lines depict the original data. Blue bars indicate $\delta^{13}C$ minimum events during glacial terminations and the Marine Isotope Stage (MIS) 4/3 transition. MIS are indicated at the top of the panel a.

5.2. Mechanisms behind $\delta^{13}C$ minimum events at thermocline and intermediate depth

5.2.1. The oceanic tunnel hypothesis

The deglacial $\delta^{13}C$ minimum events shown by our records can be potentially explained by the transport of ^{13}C-depleted carbon from the deep ocean to the SO surface and its equatorward advection by SOIWs (Spero and Lea, 2002), the so-called “oceanic tunnel” hypothesis (e.g., Pena et al., 2013), in reference to Liu and Yang (2003). The deep ocean is hypothesized

as the main sink of atmospheric CO_2 during glacial periods. During glacial terminations, the SO warmed (WAIS members, 2013; Barker et al. 2009), the sea-ice cover shrank (WAIS members, 2013; Gersonde and Zielinski, 2000), and the Southern Hemisphere westerlies are thought to have shifted southward and strengthened (Menviel et al., 2018; Toggweiler et al., 2006). The reduction in brine rejection due to reduced sea-ice cover, together with the stronger westerlies, resulted in the breakup of deep ocean stratification and enhancement of its ventilation (Du et al., 2018; Basak et al., 2018; Skinner et al., 2010), transporting nutrient-rich and ^{13}C-depleted waters from the deep ocean to the SO surface (Anderson et al., 2009; Ziegler et al., 2013). Finally, the low $\delta^{13}C$ signal was transmitted northward by the SOIWs (Spero and Lea, 2002). Spero and Lea (2002) hypothesized a correspondence between the $\delta^{13}C_{DIC}$ signals of central waters and AAIW for the "oceanic tunnel" hypothesis to be valid. Indeed, our planktonic records share a similar structure with the benthic record from GL-1180 (Fig 2a). Since modern SACW and AAIW have a similar source and formation mechanism (Pellichero et al., 2018; Abernathey et al., 2016; Tomczak and Godfrey, 1994), our results, at least theoretically, corroborate the subsurface link between the SO and low latitudes, which resulted in the $\delta^{13}C$ minima observed in the western South Atlantic over the last three glacial terminations.

Ninnemann and Charles (1997) speculated that regions with little or no influence of SOIWs should have a different $\delta^{13}C$ signal from that seen in the Southern Hemisphere. However, $\delta^{13}C$ minima have also been found in thermocline records of the subtropical North Atlantic, far from the influence of SOIWs (Lynch-Stieglitz et al., 2019). Besides, at intermediate depth, the occurrence of these events was limited to the tropical (e.g., Poggemann et al., 2017; Freeman et al., 2015; Arz et al., 1999) and North Atlantic (e.g., Oppo et al., 2015; Rickaby and Elderfield, 2005). In contrast, intermediate depth $\delta^{13}C$ records from subtropical latitudes of the southern Brazilian margin (~27°S) revealed no evidence of ^{13}C-depleted northward-flowing AAIW during the last glacial termination (Lund et al., 2015; Tessin and Lund, 2013; Oppo and Horowitz, 2000). Analogous results were reported at intermediate depth of the eastern subtropical Pacific Ocean (Pahnke and Zahn, 2005; Bostock et al., 2004). Additionally, intermediate depth $\Delta^{14}C$ records (a proxy of water mass ventilation) from the SO do not point to a poorly

ventilated AAIW during the last termination (Burke and Robinson, 2012). Similarly, $\Delta^{14}C$ records from the southern Brazilian margin (Sortor and Lund, 2011) and equatorial Atlantic (Cléroux et al., 2011; Chen et al., 2020) give support to persistent well-ventilated thermocline and intermediate waters during Termination I. Together, stable and radiogenic carbon isotopes, suggest that the SOIWs were not a pathway for aged and ^{13}C-depleted carbon accumulated in the deep ocean during glacial periods. Therefore, the "oceanic tunnel" mechanism is not expected to have played a major role in causing the $\delta^{13}C$ minimum events in our records and in other records from the tropical and North Atlantic.

5.2.2. The thermodynamic ocean-atmosphere isotopic equilibration hypothesis

$\delta^{13}C$ minimum events in the atmosphere (Fig. 4a) (Eggleston et al., 2016; Schmitt et al., 2012) have also been ascribed to the enhanced upwelling around the Antarctica and the outgassing of ^{13}C-depleted CO_2 from the SO ocean surface (Schmitt et al., 2012). Previous studies have suggested that the atmosphere can work as a bridge, globalizing its low atmospheric $\delta^{13}C$ signal in the upper ocean through the temperature-mediated ocean-atmosphere isotopic equilibration, also named thermodynamic equilibration (Shao et al., 2021; Lynch-Stieglitz et al., 2019). Accordingly, the deglacial $\delta^{13}C$ minima observed in thermocline and intermediate depths in the western South Atlantic (Fig. 2a) may have been caused by the thermodynamic equilibration in the formation regions of the water masses that fill these depths (Lynch-Stieglitz et al. 2019; Lynch-Stieglitz et al., 1995; Lynch-Stieglitz and Fairbanks, 1994; Broecker and Maier-Reimer, 1992). This hypothesis explains, for example, the presence of low $\delta^{13}C$ signal in oceanic regions where the nutrient concentrations are thought to have been always low and in regions that are not affected by the northward flowing SOIWs, as the North Atlantic (Lynch-Stieglitz et al., 2019; Ninnemann and Charles, 1997).

Empirical experiments indicate that the $\delta^{13}C$ at the ocean surface tend to be 0.1 ‰ higher relative to the atmospheric value per degree of cooling (Zhang et al., 1995). To estimate the influence of the thermodynamic equilibration in the western South Atlantic, we used the sea surface temperature (SST) record from site GL-1090 (Fig. 4b) (Santos et al., 2017) and

the isotopic composition of atmospheric CO_2 over the last 150 kyr (Fig. 4a) (Eggleston et al., 2016) to estimate the predicted $\delta^{13}C_{DIC}$ at the ocean surface. We applied the thermodynamic isotopic-equilibrium equation published by Zhang et al. (1995), where $\varepsilon_{DIC\text{-}g}$ = (10.51 $\pm$ 0.05) - (0.105 $\pm$ 0.002) $\times$ T. This equation was derived from direct measurement of the isotope fractionation between DIC of seawater and atmospheric CO_2 for a temperature and carbonate ion fraction range of 5 to 25°C and 0.05 to 0.2, respectively (Zhang et al., 1995). By using the SST record from GL-1090 (24°S), we assume that this region in the South Atlantic Subtropical Gyre is representative of where the ocean exchanges CO_2 with the atmosphere and that these surface waters will be eventually pumped to the South Atlantic thermocline. It is also noteworthy that this estimate only assumes the effect of thermodynamic equilibration on the $\delta^{13}C_{DIC}$. The predicted $\delta^{13}C_{DIC}$ (Fig. 4d) strongly resembles the *G. inflata* $\delta^{13}C$ record (Fig. 4c), showing similar millennial and long-term variations and with similar magnitude of $\delta^{13}C$ drops to those presented by our planktonic foraminifera record. Therefore, we argue that the ocean-atmospheric thermodynamic equilibration can substantially modulate the thermocline $\delta^{13}C$ in the western South Atlantic in orbital time-scales. Indeed, this result agrees with recent numerical modeling, which demonstrates that thermodynamic equilibration dominates the upper ocean $\delta^{13}C_{DIC}$ minimum anomaly during the last glacial termination (Shao et al., 2021). Previous modeling outputs also support the role of thermodynamic equilibration on the upper ocean $\delta^{13}C_{DIC}$ (Menviel et al., 2018; Schmittner and Lund, 2015).

The average of our predicted $\delta^{13}C_{DIC}$ record (1.48 ‰) is ~0.7 ‰ higher relative to the average of our *G. inflata* $\delta^{13}C$ record (0.8 ‰). This result is expected since $\delta^{13}C_{DIC}$ was predicted for the ocean surface. Additionally, as mentioned in section 5.1., *G. inflata* $\delta^{13}C$ shows a negative offset relative to $\delta^{13}C_{DIC}$ (e.g., Wilke et al., 2006). Besides, the thermocline $\delta^{13}C_{DIC}$ in the western tropical and South Atlantic is also affected by the $\delta^{13}C$ signal of the remineralized and preformed components of DIC (Oppo et al., 2018).

Both the predicted and the *G. inflata* $\delta^{13}C$ records show a remarkable drop (~0.5 ‰) during the MIS 4/3 transition (Fig. 4c, d). This drop is similar to that found in $\delta^{13}C$ of atmospheric CO_2 (~0.5 ‰) (Eggleston et al., 2016). The MIS 4/3 transition can be considered an unfinished glacial termination following the maximum extension of Southern Hemisphere glaciers at ~65 ka (MIS 4) (Schaefer et al., 2015). Indeed, several lines of evidence point to the Southern Hemisphere under full glacial conditions during MIS 4 (Kohfeld and Chase, 2017; Schaefer et al., 2015; Barker and Diz, 2014). During MIS 4/3 transition, Antarctica showed a substantial warming, equivalent to the beginning of a full glacial termination (Wolff et al., 2009). In addition, the atmospheric CO_2 concentration increased by ~30 ppm (Bereiter et al. 2012). We argue that the climatic conditions around MIS 4/3 transition were akin to the beginning of a full termination. Consequently, the enhancement of the SO upwelling during this transition resulted in the transfer of ^{13}C-depleted carbon from the deep ocean to the atmosphere, which ultimately imprinted its signal in the upper ocean.

A reduction of the biological pump efficiency may also have contributed to the negative $\delta^{13}C$ anomaly in the thermocline during glacial terminations, due to the accumulation of isotopically light carbon in the upper ocean (Lund et al., 2019; Hertzberg et al., 2016; Schmittner and Lund, 2015). However, $\delta^{13}C$ depletions are observed in regions where changes in the biological pump are not expected to have occurred, e.g., site GL-1180 (8°S), which is in the northern portion of the oligotrophic South Atlantic Subtropical Gyre. We also found thermocline $\delta^{13}C$ depletions in regions where the primary productivity is thought to have increased during the last termination, as indicated by Pereira et al. (2018) for the region of sediment core GL-1090 (24°S). However, a weaker biological pump at the Subantarctic Zone (SAZ), due to reduced dust-borne iron supply during Termination I (Martínez-García et al., 2014; Jaccard et al., 2013), may have caused the advection of ^{12}C-enriched waters to the western South Atlantic. These changes in the biological pump at the SAZ can be particularly relevant to the thermocline $\delta^{13}C_{DIC}$ depletion in the domain of SAMW, but it would have minimal influence on the thermocline $\delta^{13}C$ minima seen in the Northern Hemisphere (e.g., Lynch-Stieglitz et al., 2019).

Although the thermodynamic equilibration may have provided a substantial contribution to the thermocline $\delta^{13}C_{DIC}$ minimum during glacial terminations, the absence of a ^{13}C-depleted signal at intermediate depth in the South Brazilian margin (27°S) (Tessin and Lund, 2013; Lund et al., 2015) implies that the isotopic equilibration through southern-sourced waters did not imprint the low $\delta^{13}C_{DIC}$ signal at intermediate depth of the South Atlantic. Alternatively, the signal of the thermodynamic equilibration in AAIW may have been overcome by other processes. For example, a weaker biological pump at the SAZ may have reduced the export of organic matter and its remineralization at intermediate depth, thus causing the increase in the $\delta^{13}C_{DIC}$ observed in the AAIW domain (Hertzberg et al., 2016). Such a hypothesized reduction of the biological pump at the SAZ agrees with the role of the regeneration of organic matter in modulating the $\delta^{13}C_{DIC}$ signal at intermediate depth of the tropical and South Atlantic, as shown by Oppo et al. (2018).

Therefore, in agreement with previous studies (e.g., Shao et al., 2021; Lynch-Stieglitz et al., 2019) we suggest that the atmosphere acted as a bridge during the early deglaciation, spreading the $\delta^{13}C$ minimum signal globally in the upper ocean. Although thermodynamic equilibration may have modulated the $\delta^{13}C_{DIC}$ minimum events, changes in preformed and remineralized components of DIC can also affect $\delta^{13}C_{DIC}$, particularly in the domain of SAMW (Oppo et al., 2018). Finally, in the South Atlantic, the signal of thermodynamic equilibration was mostly seen in the thermocline so that an alternative mechanism and/or pathway is warranted to explain the $\delta^{13}C$ minimum events observed in the benthic $\delta^{13}C$ record from GL-1180 (1037 m, 8° S).

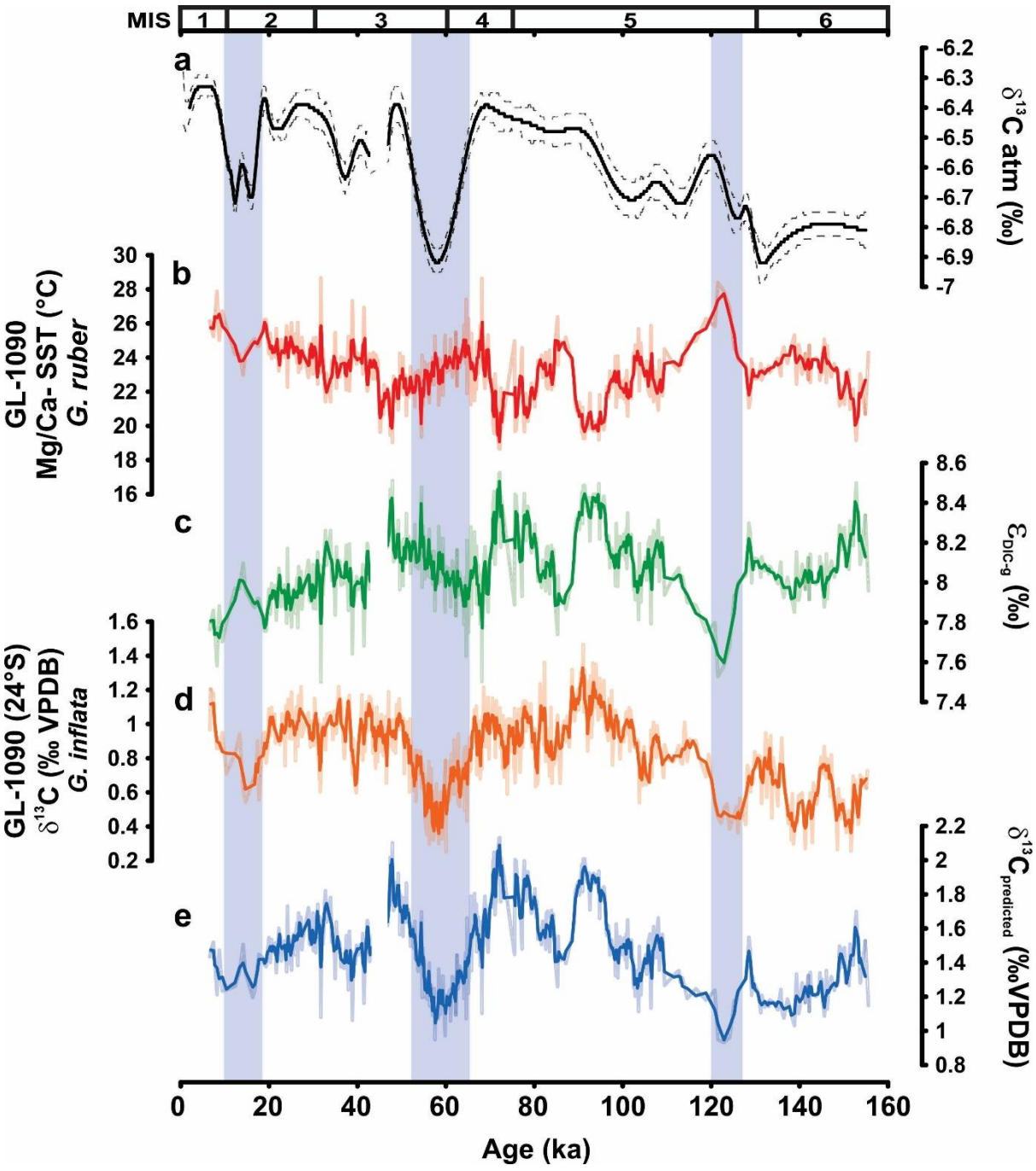

Figure 4. Effect of temperature dependent ocean-atmosphere isotopic equilibration on the stable carbon isotope ratio of the dissolved inorganic carbon ($\delta^{13}C_{DIC}$) of ocean surface in site GL-1090. a) Monte Carlo cubic spline average of atmospheric $\delta^{13}C$ over the last 150 kyr (Eggleston et al., 2016); b) Mg/Ca based sea surface temperature from sediment core GL-1090 (Santos et al. 2017), SST was recalculated using Mg/Ca-temperature equation from Gray and Evans (2019). c) The ^{13}C fractionation between ocean DIC and atmosphere CO_2 calculated using the equation from Zhang et al. (1995). d) $\delta^{13}C$ of *Globorotalia inflata* from site GL-1090

(this study). e) The predicted $\delta^{13}C_{DIC}$ of ocean surface assuming the thermodynamic ocean-atmosphere isotopic equilibration. Bars indicates times synchronic $\delta^{13}C$ drops in the predicted $\delta^{13}C_{DIC}$ and *G. inflata* $\delta^{13}C$. The thick lines in panels b, c, d, and e depict 3-points running averages.

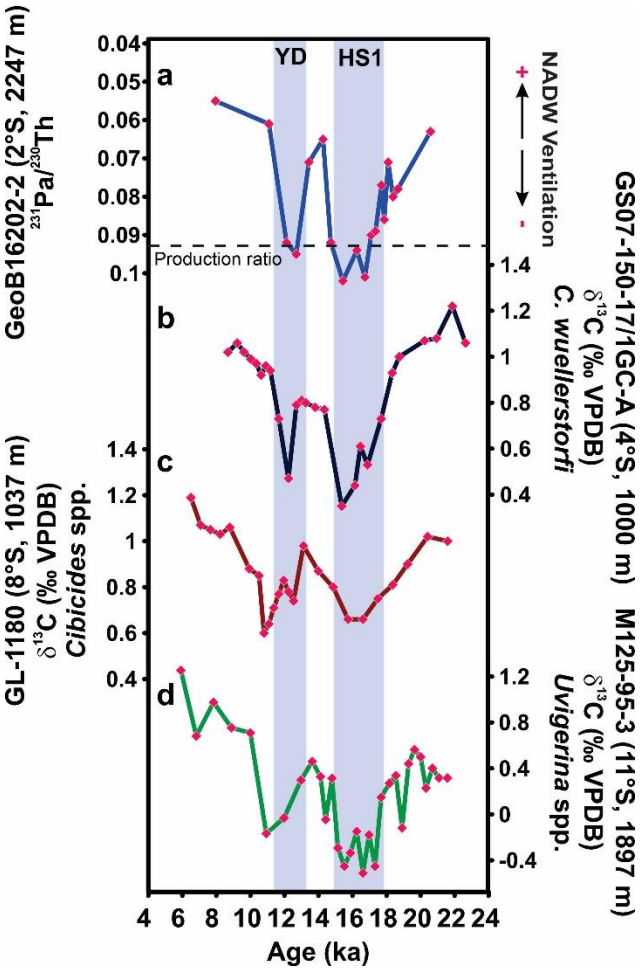

Figure 5. Comparison between the stable carbon isotopic composition ($\delta^{13}C$) of benthic foraminifera from intermediate and mid-depth of the South Atlantic and radiochemical data from the North Atlantic. a) $^{231}Pa/^{230}Th$ record from sediment core GeoB16206-1 (Mulitza et al. 2017). Note inverted y axis. b) Benthic $\delta^{13}C$ from sediment core GS07-150-17/1GC-A (Freemann et al., 2015). c) Benthic $\delta^{13}C$ of sediment core GL-1180 (this study). d) Benthic $\delta^{13}C$ of sediment core M125-95-3 (Campos et al., 2020). Blue bars indicate Heinrich Stadial 1 (HS1) and the Younger Dryas (YD).

5.2.3. $\delta^{13}C$ minimum events at intermediate depth of the tropical Atlantic: the AMOC slowdown hypothesis

As discussed in sections 5.2.1 and 5.2.2, neither the "oceanic tunnel" nor thermodynamic equilibration through southern-sourced waters can explain the $\delta^{13}C$ minimum events observed in our GL-1180 benthic $\delta^{13}C$ record. Here we point to a North Atlantic origin of $\delta^{13}C$ minimum events at the intermediate depth of the tropical Atlantic. Over the last glacial termination, ^{13}C-depleted waters have been observed in the mid-depth of the North, tropical, and South Atlantic (Campos et al., 2020; Lacerra et al., 2017; Voigt et al., 2017; Oppo et al., 2015; Lund et al., 2015; Tessin and Lund, 2013). This depletion is likely linked to the reduced NADW ventilation rate during Heinrich Stadial 1 and the Younger Dryas, resulting in the accumulation of respired carbon at mid-depth of the Atlantic Ocean (Lacerra et al., 2017; Schmittner and Lund, 2015). Indeed, reduced NADW ventilation rate is supported by $^{231}Pa/^{230}Th$ values (Fig. 5a) from mid-depth of the Atlantic Ocean (e.g., Mulitza et al. 2017; Voigt et al. 2017). Accordingly, this mid-depth ^{13}C-depleted signal could have affected intermediate depth (~1000 m) $\delta^{13}C_{DIC}$ signal at the Brazilian equatorial margin during Termination I, as observed in benthic $\delta^{13}C$ record (Fig. 5b) from site GS07-150-17/1GC-A (Fig. 1) (Freeman et al., 2015).

Numerical modeling supports a decrease of $\delta^{13}C_{DIC}$ from the surface to mid-depth of the Atlantic Ocean during periods of AMOC slowdown, although this decrease is more expressive at intermediate and mid-depths of the tropical and North Atlantic (Menviel et al., 2018; Schmittner and Lund, 2015). These simulations agree with $\delta^{13}C$ records of benthic foraminifera (e.g., Campos et al., 2020; Voigt et al., 2017; Oppo et al., 2015). Therefore, we suggest that the $\delta^{13}C$ depletion observed at intermediate depth of the western tropical South Atlantic (e.g., site GL-1180) was likely caused by the reduction of the North Atlantic overturning and accumulation of isotopically light carbon at intermediate and mid-depths. Indeed, over the last deglaciation, our benthic $\delta^{13}C$ record (Fig. 5c) presents the same "W-like" shape observed in benthic $\delta^{13}C$ record of core M125-95-3 (Fig. 5d), collected from the mid-depth of the tropical South Atlantic (Fig. 1) (Campos et al., 2020). The early $\delta^{13}C$ decrease in the GL-1180 benthic record relative to other benthic records shown in Fig. 5 may result from the limited chronologic

control (6 radiocarbon ages) and the lower sampling resolution of GL-1180 over the early deglaciation. No substantial chronological difference is found by calibrating the radiocarbon ages of GL-1180 with the Marine20 calibration curve (Heaton et al. 2020) (Supporting Information, Text S2). Given the location and resemblance of GL-1180 benthic record relative to sediment cores M125-95-3 (Campos et al., 2020) and GS07-150-17/1GC-A (Freeman et al., 2015) (Fig. 1 and Fig. 5), it is reasonable to assume that over the Termination I, the bottom of the water column at these sites were influenced by a $\delta^{13}C$ signal of similar origin. Together, these results support that the ^{13}C-depletion at intermediate depth of the tropical Atlantic is mostly caused by the aged North Atlantic sourced waters. This interpretation can be applied to $\delta^{13}C$ minimum events that occurred during previous glacial terminations, as seen in our benthic record (Fig. 2a). Importantly, this hypothesis is dissociated from the "ocean tunnel" and the ocean-atmosphere isotopic equilibration.

However, it has also been hypothesized that the thermodynamic equilibration could be equally responsible for the $\delta^{13}C$ minimum observed at mid-depth of the Atlantic Ocean over the last termination by affecting the formation region of the NADW (Lynch-Stieglitz et al., 2019). However, a recent study showed that mid-depth benthic $\delta^{13}C$ minimum leads the planktonic counterpart and atmospheric $\delta^{13}C$ by ~800 years (Lund et al., 2019). If the ocean-atmosphere isotopic equilibration was responsible for $\delta^{13}C$ minimum at mid-depth of the Atlantic Ocean, one would expect the atmosphere to lead the ocean. Therefore, the lag of the atmosphere relative to the ocean implies that the ocean-atmosphere isotopic equilibration through northern-sourced waters is unlikely to have been the main driver of the $\delta^{13}C$ minimum event at intermediate and mid-depths of the Atlantic Ocean during Termination I.

In contrast to our reasoning of a northern-sourced $\delta^{13}C$ minimum at intermediate depth, Poggemann et al. (2017) suggested an injection of nutrient-rich ^{13}C-depleted AAIW at intermediate depth of the tropical North Atlantic during the last deglaciation (site M78/1-235-1; Fig. 1). This conclusion was based on benthic $\delta^{13}C$ and seawater-dissolved cadmium (Cd_w), a proxy for phosphate concentration in seawater. However, as stressed above, the low $\delta^{13}C$

signal contradicts depth transects from the southern Brazilian margin (Lund et al., 2015; Tessin and Lund, 2013; Oppo and Horowitz, 2000). While part of this Cd_w increase shown by Poggemann et al. (2017) may result from the remineralization of organic matter and nutrient accumulation due to the AMOC slowdown, another part must be decoupled from the $\delta^{13}C_{DIC}$ since records from the upper North Atlantic show that increases in Cd_w are not simultaneous with $\delta^{13}C$ decreases (Lynch-Stieglitz et al., 2019). Indeed, a recent study showed that although the $\delta^{13}C_{DIC}$ signal of upwelled deep waters is strongly affected by ocean-atmosphere isotopic equilibration in the SO surface, nutrients are still transported northward through the "oceanic tunnel" decoupled from $\delta^{13}C_{DIC}$ signal (Shao et al., 2021). Therefore, this result can help to conciliate Cd_w and benthic $\delta^{13}C$ records from intermediate depth of the tropical Atlantic.

6. Conclusions

We present three high temporal resolution thermocline and intermediate depth (1037 m) foraminiferal $\delta^{13}C$ records from the western South Atlantic spanning the last 300 kyr. The planktonic and benthic records show remarkable $\delta^{13}C$ minimum events during the last three glacial terminations, as well as during the MIS 4/3 transition. Benthic $\delta^{13}C$ depth transects from the south Brazilian margin, as well as intermediate depth $\delta^{13}C$ records from the Pacific Ocean, contradict the long-held hypothesis of a northward advection of ^{13}C-depleted carbon from the SO surface by SAMW and AAIW. Instead, we suggest that the $\delta^{13}C$ minima at the thermocline and intermediate depths were governed by two distinct and independent mechanisms. The good correspondence between predicted $\delta^{13}C_{DIC}$ and planktonic $\delta^{13}C$ from the southern Brazilian margin indicates that the thermodynamic ocean-atmosphere isotopic equilibration strongly modulated the $\delta^{13}C_{DIC}$ signal in the western South Atlantic thermocline. This mechanism can explain the global occurrence of $\delta^{13}C$ minimum events in the upper ocean and agrees with recent numerical modeling. Indeed, the thermodynamic equilibration is a leading driver of the ^{13}C-depleted signal in the western South Atlantic thermocline during glacial terminations and MIS 4/3 transition. However, in the domain of SAMW, changes in the biological pump in the SAZ must also be considered. We propose that the origin of the $\delta^{13}C$ minimum

events at intermediate depths of the tropical Atlantic is related to the slow rate of NADW formation during glacial terminations and the accumulation of remineralized carbon at mid and intermediate depths of the tropical and North Atlantic. Importantly, the latter mechanism does not evoke the deep ocean and upwelling in the SO as a source of ^{13}C-depleted carbon to intermediate depths of the Atlantic Ocean.

Data availability

All data presented in the manuscript are available at [LINK]

Acknowledgments

We thank the two anonymous reviewers for their comments and suggestions that improved the manuscript. We also thank Petrobras for providing the sediment core used in this study. This study was supported by the CAPES-ASpECTO project (grant 88887.091731/2014-01) CNPq-Aspecto (grant 429767/2018-8), CAPES-PRINT CLIMATE Project (grant 88887.310301/2018-00) and CNPq Project RAiN (grant 406322/2018-0). R.A.N. acknowledges the scholarship from CAPES (grant 88887.176103/2018-00). CAPES also financially supported I.M.V. with a scholarship (grant 88887.156152/2017-00). C.M.C. acknowledges the financial support from FAPESP (grants 2018/15123-4 and 2019/24349-9), CAPES (grants 564/2015 and 88881.313535/2019-01), CNPq (grants 302607/2016-1 and 312458/2020-7), and the Alexander von Humboldt Foundation. R.C.P.-R acknowledges the financial support from the European Union's Horizon 2020 iAtlantic project (grant 818123). B.B.D. appreciates financial support from FAPESP (2020/11452-3). T.M.L. Pinho acknowledges the financial support from FAPESP (grant 2019/10642-6). A.L.S.A. is a senior scholar CNPq (grant 302521/2017-8). We also acknowledge the partial support from the Coordenação de Aperfeiçoamento de Pessoal de Nível Superior – Brasil (CAPES) – Finance Code 001. This is LSCE publication number 7732. All data presented in this manuscript is available at https://doi.org/10.1594/PANGAEA.936785.

References

618 Abernathey, R.P., Cerovecki, I., Holland, P.R., Newsom, E., Mazloff, M., Talley, L.D., (2016).
619 Water-mass transformation by sea ice in the upper branch of the Southern Ocean overturning.
620 Nat. Geosci. 9, 596–601. https://doi.org/10.1038/ngeo2749

621 Anderson, R.F., Ali, S., Bradtmiller, L.I., Nielsen, S.H.H., Fleisher, M.Q., Anderson, B.E.,
622 Burckle, L.H., (2009). Wind-Driven Upwelling in the Southern Ocean and the Deglacial Rise
623 in Atmospheric CO^2. Science, 323, 1443–1448. https://doi.org/1126/science.1167441

624 Arz, H. W., Pätzold, J., Wefer, G. (1999). The deglacial history of the western tropical Atlantic
625 as inferred from high resolution stable isotope records off northeastern Brazil, Earth Planet.
626 Sci. Lett., 167, 105–117, doi:10.1016/S0012-821X(99)00025-4.

627 Ballalai, J.M., Santos, T.P., Lessa, D.O., Venancio, I.M., Chiessi, C.M., Johnstone, H.J.H.,
628 Kuhnert, H., Claudio, M.R., Toledo, F., Costa, K.B., Albuquerque, A.L.S., (2019). Tracking
629 spread of the Agulhas leakage into the western South Atlantic and its northward transmission
630 during the last interglacial. Paleoceanogr. Paleoclimatol., 34(11), 1744-
631 1760. https://doi.org/10.1029/2019PA003653;

632 Barker, S., Diz, P., (2014). Timing of the descent into the last Ice Age determined by the bipolar
633 seesaw. Paleoceanography, 29, 489–507. https://doi.org/10.1002/2014PA002623

634 Barker, S., Diz, P., Vautravers, M.J., Pike, J., Knorr, G., Hall, I.R., Broecker, W.S., (2009).
635 Interhemispheric Atlantic seesaw response during the last deglaciation. Nature, 457, 1097–
636 1102. https://doi.org/10.1038/nature07770

637 Basak, C., Fröllje, H., Lamy, F., Gersonde, R., Benz, V., Anderson, R.F., Molina-Kescher, M.,
638 Pahnke, K., 2018. Breakup of last glacial deep stratification in the South Pacific. Science, 359,
639 900–904. https://doi.org/10.1126/science.aao2473

640 Bemis, B.E., Spero, H.J., Lea, D.W., Bijma, J., (2000). Temperature influence on the carbon
641 isotopic composition of *Globigerina bulloides* and *Orbulina universa* (planktonic foraminifera).
642 Mar. Micropaleontol., 38, 213–228. https://doi.org/10.1016/S0377-8398(00)00006-2

643 Bereiter, B., Lüthi, D., Siegrist, M., Schüpbach, S., Stocker, T.F., Fischer, H., (2012). Mode
644 change of millennial CO_2 variability during the last glacial cycle associated with a bipolar ma-
645 rine carbon seesaw. Proc. Natl. Acad. Sci. U. S. A., 109, 9755–9760.
646 https://doi.org/10.1073/pnas.1204069109

647 Birch, H., Coxall, H.K., Pearson, P.N., Kroon, D., O'Regan, M., (2013). Planktonic
648 foraminifera stable isotopes and water column structure: disentangling ecological signals. Mar.
649 Micropaleontol., 101, 127–145. https://doi.org/10.1016/j.marmicro.2013.02.002;

650 Blaauw, M. (2010). Methods and code for "classical" age-modelling of radiocarbon sequences.
651 Quat. Geochronol., 5(5), 512–518. http://doi.org/10.1016/j.quageo.2010.01.002

652 Blaauw, M., Christen, J. A. (2011). Flexible paleoclimate age-depth models using an auto-
653 regressive gamma process. Bayesian Anal., 6(3), 457–474. https://doi.org/10.1214/11-
654 BA618;

655 Bostock, H.C., Opdyke, B.N., Gagan, M.K. and Fifield, L.K., (2004). Carbon isotope evidence
656 for changes in Antarctic Intermediate Water circulation and ocean ventilation in the southwest
657 Pacific during the last deglaciation. Paleoceanography, 19(4).
658 https://doi.org/10.1029/2004PA001047

659 Broecker, W.S., Maier-Reimer, E., (1992). The influence of air and sea exchange on the
660 carbon isotope distribution in the sea. Glob. Biogeochem. Cycles 6, 315–320.
661 https://doi.org/10.1029/92GB01672

662 Burke, A., Robinson, L.F., (2012). The southern ocean's role in carbon exchange during the
663 last deglaciation. Science, 335, 557–561. https://doi.org/10.1126/science.1208163

Campos, M.C., Chiessi, C.M., Venancio, I.M., Pinho, T.M.L., Crivellari, S., Kuhnert, H., Schmiedl, G., Díaz, R.A., Albuquerque, A.L.S., Portilho-Ramos, R.C., Bahr, A., Mulitza, S., (2020). Constraining Millennial-Scale Changes in Northern Component Water Ventilation in the Western Tropical South Atlantic, Paleoceanogr. Paleoclimatol.. https://doi.org/10.1029/2020PA003876

Chen, T., Robinson, L.F., Burke, A., Claxton, L., Hain, M.P., Li, T., Rae, J.W., Stewart, J., Knowles, T.D., Fornari, D.J. and Harpp, K.S., 2020. Persistently well-ventilated intermediate-depth ocean through the last deglaciation. Nat. Geosci., 13(11), pp.733-738. https://doi.org/10.1038/s41561-020-0638-6

Chiessi, C.M., Ulrich, S., Mulitza, S., Pätzold, J., Wefer, G. (2007). Signature of the Brazil-Malvinas Confluence (Argentine Basin) in the isotopic composition of planktonic foraminifera from surface sediments. Mar. Micropaleontol., 64, 52–66. https://doi.org/10.1016/j.marmicro.2007.02.002;

Cléroux, C., Cortijo, E., Duplessy, J.C., Zahn, R. (2007). Deep-dwelling foraminifera as thermocline temperature recorders. Geochem. Geophys. Geosys., 8(4). https://doi.org/10.1029/2006GC001474;

Cléroux, C., deMenocal, P. and Guilderson, T., 2011. Deglacial radiocarbon history of tropical Atlantic thermocline waters: absence of CO2 reservoir purging signal. Quat. Sci. Rev., 30(15-16), pp.1875-1882. https://doi.org/10.1016/j.quascirev.2011.04.015

Cléroux, C., Demenocal, P., Arbuszewski, J., Linsley, B., (2013). Reconstructing the upper water column thermal structure in the Atlantic Ocean. Paleoceanography 28, 503–516. https://doi.org/10.1002/palo.20050

Crivellari, S., Viana, P.J., Campos, M.C., Kuhnert, H., Barros, A., Cruz, F.W., Chiessi, C.M., (2021). Development and characterization of a new in-house reference material for stable carbon and oxygen isotopes analyses. Journal of Analytical Atomic Spectrometry. DOI 10.1039/D1JA00030F

Curry, W.B., Oppo, D.W., (2005). Glacial water mass geometry and the distribution of $\delta^{13}C$ of ΣCO_2 in the western Atlantic Ocean. Paleoceanography 20, 1–12. https://doi.org/10.1029/2004PA001021

Du, J., Haley, B.A., Mix, A.C., Walczak, M.H., Praetorius, S.K., (2018). Flushing of the deep Pacific Ocean and the deglacial rise of atmospheric CO_2 concentrations. Nat. Geosci. 11, 749–755. https://doi.org/10.1038/s41561-018-0205-6

Eggleston, S., Schmitt, J., Bereiter, B., Schneider, R., Fischer, H., (2016). Evolution of the stable carbon isotope composition of atmospheric CO_2 over the last glacial cycle. Paleoceanography 31, 434–452. https://doi.org/10.1002/2015PA002874

Eide, M., Olsen, A., Ninnemann, U.S., Johannessen, T., (2017). A global ocean climatology of preindustrial and modern ocean $\delta^{13}C$. Glob. Biogeochem. Cycles 31, 515–534. https://doi.org/10.1002/2016GB005473

Elderfield, H., Vautravers, M., Cooper, M., (2002). The relationship between shell size and Mg/Ca, Sr/Ca, $\delta^{18}O$, and $\delta^{13}C$ of species of planktonic foraminifera. Geochem. Geophys. Geosys., 3, 1–13. https://doi.org/10.1029/2001gc000194

Emery, W., Meincke, J., (1986). Global water masses: summary and review. Oceanol. Acta, 9, 383–391.

England, M.H., Godfrey, J.S., Hirst, A.C., Tomczak, M., 1993. The mechanism for Antarctic Intermediate Water renewal in a world ocean model. J. Phys. Oceanogr., *23*(7), 1553-1560. https://doi.org/10.1175/1520 0485(1993)023<1553:TMFAIW>2.0.CO;2

710 Farmer, E.C., Kaplan, A., de Menocal, P.B., Lynch-Stieglitz, J., (2007). Corroborating ecolog-
711 ical depth preferences of planktonic foraminifera in the tropical Atlantic with the stable oxygen
712 isotope ratios of core top specimens. Paleoceanography 22, 1–14.
713 https://doi.org/10.1029/2006PA001361

714 Feldmeijer, W., Metcalfe, B., Brummer, G., Ganssen, G. (2014). Reconstructing the depth of
715 the permanent thermocline through the morphology and geochemistry of the deep dwelling
716 planktonic foraminifer *Globorotalia truncatulinoides*. Paleoceanography, 30, 1–22.
717 https://doi.org/10.1002/2014PA002687

718 Freeman, E., Skinner, L.C., Tisserand, A., Dokken, T., Timmermann, A., Menviel, L., Friedrich,
719 T., (2015). An Atlantic-Pacific ventilation seesaw across the last deglaciation. Earth Planet.
720 Sci. Lett. 424, 237–244. https://doi.org/10.1016/j.epsl.2015.05.032

721 Friedrich, O., Schiebel, R., Wilson, P.A., Weldeab, S., Beer, C.J., Cooper, M.J., Fiebig, J.,
722 (2012). Influence of test size, water depth, and ecology on Mg/Ca, Sr/Ca, $\delta^{18}O$ and $\delta^{13}C$ in
723 nine modern species of planktic foraminifers. Earth Planet. Sci. Lett. 319–320, 133–145.
724 https://doi.org/10.1016/j.epsl.2011.12.002

725 Gebbie, G. (2014). How much did glacial North Atlantic water shoal? Paleoceanography, 29,
726 190‐209. https://doi.org/10.1002/2013PA002557

727 Gersonde, R. and Zielinski, U., (2000). The reconstruction of late Quaternary Antarctic sea-
728 ice distribution—the use of diatoms as a proxy for sea-ice. Palaeogeogr. Palaeoclimatol. Pa-
729 laeoecol., 162(3-4), 263-286. https://doi.org/10.1016/S0031-0182(00)00131-0

730 Gray, W.R., Evans, D., (2019). Nonthermal Influences on Mg/ca in Planktonic
731 Foraminifera: a Review of Culture Studies and Application to the last Glacial
732 Maximum. Paleoceanogr. Paleoclimatol. 34, 306‐315. https://doi.org/10.1029/
733 2018PA003517.

734 Gordon, A.L., (1986). Interocean exchange of thermocline water. Journal of Geophysical Re-
735 search, 91, 5037-5046. https://doi.org/10.1029/JC091iC04p05037

736 Govin, A., Capron, E., Tzedakis, P.C., Verheyden, S., Ghaleb, B., Hillaire-Marcel, C., St-Onge,
737 G., Stoner, J.S., Bassinot, F., Bazin, L., Blunier, T., (2015). Sequence of events from the onset
738 to the demise of the Last Interglacial: Evaluating strengths and limitations of chronologies used
739 in climatic archives. Quat. Sci. Rev., 129, 1–36. http://doi.org/10.1016/j.quasci-
740 rev.2015.09.018;

741 Govin, A., Chiessi, C.M., Zabel, M., Sawakuchi, A.O., Heslop, D., Hörner, T.,
742 Zhang, Y., Mulitza, S., (2014). Terrigenous input off northern South America driven by
743 changes in Amazonian climate and the North Brazil Current retroflection during the last 250
744 ka. Clim. Past 10, 843–862. http://dx.doi.org/ 10.5194/cp-10-843-2014.

745 Groeneveld, J., Chiessi, C.M., (2011). Mg/Ca of *Globorotalia inflata* as a recorder of perma-
746 nent thermocline temperatures in the South Atlantic. Paleoceanography 26, 1–12.
747 https://doi.org/10.1029/2010PA001940

748 Heaton, T.J., Köhler, P., Butzin, M., Bard, E., Reimer, R.W., Austin, W.E., Ramsey, C.B.,
749 Grootes, P.M., Hughen, K.A., Kromer, B. and Reimer, P.J., 2020. Marine20—the marine radi-
750 ocarbon age calibration curve (0–55,000 cal BP). *Radiocarbon*, *62*(4), pp.779-820.
751 https://doi.org/10.1017/RDC.2020.68

752 Hertzberg, J.E., Lund, D.C., Schmittner, A., Skrivanek, A.L., (2016). Evidence for a biological
753 pump driver of atmospheric CO_2 rise during Heinrich Stadial 1. Geophys. Res. Lett. 43,
754 12,242-12,251. https://doi.org/10.1002/2016GL070723

755 Hodell, D.A., Venz, K.A., Charles, C.D., Ninnemann, U.S., (2003). Pleistocene vertical carbon
756 isotope and carbonate gradients in the South Atlantic sector of the Southern Ocean, Geo-
757 chem. Geophys. Geosys., 4, 1–19. https://doi.org/10.1029/2002GC000367

Howe, J.N.W., Piotrowski, A.M., Noble, T.L., Mulitza, S., Chiessi, C.M., Bayon, G., (2016a). North Atlantic Deep Water Production during the Last Glacial Maximum. Nat. Commun. 7, 1–8. https://doi.org/10.1038/ncomms11765

Hu, R., Bostock, H.C., Greaves, M., Piotrowski, A.M., McCave, I.N., (2020). Coupled evolution of stable carbon isotopes between the Southern Ocean and the atmosphere over the last 260 ka. Earth Planet. Sci. Lett. 538, 116215. https://doi.org/10.1016/j.epsl.2020.116215

Jaccard, S.L., Hayes, C.T., Martinez-Garcia, A., Hodell, D.A., Anderson, R.F., Sigman, D.M. and Haug, G.H., 2013. Two modes of change in Southern Ocean productivity over the past million years. Science, 339(6126), pp.1419-1423. https://doi.org/10.1126/science.1227545

Kohfeld, K.E.,Chase, Z., (2017). Temporal evolution of mechanisms controlling ocean carbon uptake during the last glacial cycle. Earth Planet. Sci. Lett., 472, 206-215. https://doi.org/10.1016/j.epsl.2017.05.015

Lacerra, M., Lund, D., Yu, J., Schmittner, A., (2017). Carbon storage in the mid-depth Atlantic during millennial-scale climate events. Paleoceanography 32, 780–795. https://doi.org/10.1002/2016PA003081

LeGrande, A.N., Lynch-Stieglitz, J., Farmer, E.C., (2004). Oxygen isotopic composition of *Globorotalia truncatulinoides* as a proxy for intermediate depth density. Paleoceanography, 19, PA4025. https://doi.org/10,1029/2004PA001045

Liu, Z. and Yang, H., (2003). Extratropical control of tropical climate, the atmospheric bridge and oceanic tunnel, Geophys. Res. Lett, 30, 1230, doi:10.1029/2002GL016492

Lisiecki, L. E., Raymo, M. E. (2005). A Pliocene-Pleistocene stack of 57 globally distributed benthic $\delta^{18}O$ records. Paleoceanography, *20*(1), 1–17. https://doi.org/10.1029/2004PA001071

781 Lund, D., Hertzberg, J., Lacerra, M., (2019). Carbon isotope minima in the South Atlantic dur-
782 ing the last deglaciation: Evaluating the influence of air-sea gas exchange. Environ. Res. Lett.
783 14. https://doi.org/10.1088/1748-9326/ab126f

784 Lund, D.C., Tessin, A.C., Hoffman, J.L., Schmittner, A., (2015). Southwest Atlantic water mass
785 evolution during the last deglaciation. Paleoceanography 30, 477–494.
786 https://doi.org/10.1002/2014PA002657

787 Lynch-Stieglitz, J., R.G. Fairbanks (1994). A conservative tracer for glacial ocean circulation
788 from carbon isotope and paleo-nutrient measurements in benthic foraminifera. Nature, 369,
789 308-310. https://doi.org/10.1038/369308a0

790 Lynch-Stieglitz, J., Stocker, T.F., Broecker, W.S., Fairbanks, R.G., (1995). The influence of
791 air–sea exchange on the isotopic composition of oceanic carbon – observations
792 and modeling. Glob. Biogeochem. Cycles 9, 653–665. https://doi.org/10.1029/95GB02574

793 Lynch-Stieglitz, J., Valley, S.G., Schmidt, M.W., (2019). Temperature-dependent ocean–at-
794 mosphere equilibration of carbon isotopes in surface and intermediate waters over the degla-
795 ciation. Earth Planet. Sci. Lett. 506, 466–475. https://doi.org/10.1016/j.epsl.2018.11.024

796 Marshall, J., Speer, K., (2012). Closure of the meridional overturning circulation through
797 Southern Ocean upwelling. Nat. Geosci. 5, 171–180. https://doi.org/10.1038/ngeo1391

798 Martínez-Botí, M.A., Marino, G., Foster, G.L., Ziveri, P., Henehan, M.J., Rae, J.W.B., Mortyn,
799 P.G., Vance, D., (2015). Boron isotope evidence for oceanic carbon dioxide leakage during
800 the last deglaciation. Nature 518, 219–222. https://doi.org/10.1038/nature14155

801 Martínez-García, A., Sigman, D.M., Ren, H., Anderson, R.F., Straub, M., Hodell, D.A., Jac-
802 card, S.L., Eglinton, T.I. and Haug, G.H., 2014. Iron fertilization of the Subantarctic Ocean
803 during the last ice age. Science, 343(6177), pp.1347-1350. https://doi.org/10.1126/sci-
804 ence.1246848

Menviel, L., Spencer, P., Yu, J., Chamberlain, M.A., Matear, R.J., Meissner, K.J., England, M.H., (2018). Southern Hemisphere westerlies as a driver of the early deglacial atmospheric CO_2 rise. Nat. Commun. 1–12. https://doi.org/10.1038/s41467-018-04876-4

Mulitza, S., Arz, H., Kemle-von Mucke, S., Moos, C., Niebler, H.S., Pätzold, J., Segl, M. (1999). The South Atlantic carbon isotope record of planktonic foraminifera. In *Use of Proxies in Paleocanography: Examples from the South Atlantic* (ed. Fischer, G. and Wefer, G.) (Berlin: Springer), 427–445.

Mulitza, S., Dürkoop, A., Hale, W., Wefer, G., Niebler, H. S. (1997). Planktonic foraminifera as recorders of past surface-water stratification. Geology, 25(4), 335–338. https://doi.org/10.1130/0091-7613(1997)025<0335:PFAROP>2.3.CO;2;

Mulitza, S., Rühlemann, C., Bickert, T., Hale, W., Pätzold, J., Wefer, G., (1998). Late Quaternary $\delta^{13}C$ gradients and carbonate accumulation in the western equatorial Atlantic. Earth Planet. Sci. Lett. 155, 237–249. https://doi.org/10.1016/s0012-821x(98)00012-0

Mulitza, S., Chiessi, C.M., Schefuß, E., Lippold, J., Wichmann, D., Antz, B., Mackensen, A., Paul, A., Prange, M., Rehfeld, K. and Werner, M., (2017). Synchronous and proportional deglacial changes in Atlantic meridional overturning and northeast Brazilian precipitation. Paleoceanography, 32(6), pp.622-633. https://doi.org/10.1002/2017PA003084

Nascimento, R. A., Venancio, I. M., Chiessi, C. M., Ballalai, J. M., Kuhnert, H., Johnstone, H., Santos, T. P., Prange, M., Govin, A., Crivellari, S., Mulitza, S., Albuquerque, A. L. S., (2021). Tropical Atlantic stratification response to late Quaternary precessional forcing. Earth Planet. Sci. Lett., 568, 117030, https://doi.org/10.1016/j.epsl.2021.117030

NGRIP community members, 2004. High-resolution record of Northern Hemisphere climate extending into the last interglacial period. Nature 431, 147-151. https://doi.org/10.1038/nature02805

Ninnemann, U.S., Charles, C.D., (1997). Regional differences in Quaternary Subantarctic nutrient cycling: Link to intermediate and deep-water ventilation. Paleoceanography 12, 560–567. https://doi.org/10.1029/97PA01032

Oppo, D.W., Curry, W.B., McManus, J.F., (2015). What do benthic $\delta^{13}C$ and $\delta^{18}O$ data tell us about Atlantic circulation during Heinrich Stadial 1? Paleoceanography 30, 353–368. https://doi.org/10.1002/2014PA002667

Oppo, D.W., Gebbie, G., Huang, K.F., Curry, W.B., Marchitto, T.M. and Pietro, K.R., 2018. Data constraints on Glacial Atlantic water mass geometry and properties. Paleoceanogr. Paleoclimatol., 33(9), pp.1013-1034. https://doi.org/10.1029/2018PA003408

Oppo, D.W., Horowitz, M., 2000. Glacial deep-water geometry: South Atlantic benthic foraminiferal Cd/Ca and δ13C evidence. Paleoceanography, 15(2), pp.147-160. https://doi.org/10.1029/1999PA000436

Orsi, A.H., Whitworth III, T. and Nowlin Jr, W.D., (1995). On the meridional extent and fronts of the Antarctic Circumpolar Current. Deep Sea Res. Part I Oceanogr. Res. Pap., 42(5), pp.641-673. https://doi.org/10.1016/0967-0637(95)00021-W

Pahnke, K., Zahn, R., (2005). Southern Hemisphere water mass conversion linked with North Atlantic climate variability. Science, 307(5716), 1741-1746. http://doi.org/10.1126/science.1102163

Pellichero, V., Sallée, J.B., Chapman, C.C., Downes, S.M., (2018). The Southern Ocean meridional overturning in the sea-ice sector is driven by freshwater fluxes. Nat. Commun. 9. https://doi.org/10.1038/s41467-018-04101-2

Pena, L.D., Goldstein, S.L., Hemming, S.R., Jones, K.M., Calvo, E., Pelejero, C., Cacho, I., (2013). Rapid changes in meridional advection of Southern Ocean intermediate waters to the

852 tropical Pacific during the last 30kyr. Earth Planet. Sci. Lett. 368, 20–32.
853 https://doi.org/10.1016/j.epsl.2013.02.028

854 Pereira, L.S., Arz, H.W., Pätzold, J. and Portilho-Ramos, R.C., (2018). Productivity evolution
855 in the South Brazilian Bight during the last 40,000 years. Paleoceanogr. Paleoclima-
856 tol., *33*(12), 1339-1356. https://doi.org/10.1029/2018PA003406

857 Peterson, R.G., Stramma, L., (1991). Upper-level circulation in the South Atlantic Ocean 26,
858 1–73. https://doi.org/10.1016/0079-6611(91)90006-8

859 Poggemann, D., Hathorne, E.C., Nürnberg, D., Frank, M., Bruhn, I., Reißig, S., Bahr, A.,
860 (2017). Rapid deglacial injection of nutrients into the tropical Atlantic via Antarctic Intermediate
861 Water. Earth Planet. Sci. Lett. 463, 118–126. https://doi.org/10.1016/j.epsl.2017.01.030

862 Poole, R., Tomczak, M. (1999). Optimal multiparameter analysis of the water mass structure
863 in the Atlantic Ocean thermocline. Deep-Sea Res. I: Oceanographic Research Papers, 46 (11),
864 1895-1921. https://doi.org/10.1016/S0967-0637(99)00025-4;

865 Ravelo, A. C., Hillaire-Marcel, C. (2007). The use of oxygen and carbon isotopes of foraminif-
866 era in paleoceanography. Developments in marine geology, 1, 735-764.

867 Regenberg, M., Steph, S., Nürnberg, D., Tiedemann, R., Garbe-Schönberg, D. (2009). Cali-
868 brating Mg/Ca ratios of multiple planktonic foraminiferal species with $\delta^{18}O$-calcification tem-
869 peratures: Paleothermometry for the upper water column. Earth Planet. Sci. Lett., 278(3–4),
870 324–336. https://doi.org/10.1016/j.epsl.2008.12.019;

871 Reimer, P.J., Bard, E., Bayliss, A., Beck, J.W., Blackwell, P.G., Ramsey, C.B., Buck, C.E.,
872 Cheng, H., Edwards, R.L., Friedrich, M., Grootes, P.M., (2013). IntCal13 and Marine13 radio-
873 carbon age calibration curves 0–50,000 years cal BP. Radiocarbon, 55(04), 1869–1887.
874 https://doi.org/10.2458/azu_js_rc.55.16947;

875 Rickaby, R.E.M., Elderfield, H., 2005. Evidence from the high-latitude North Atlantic for varia-
876 tions in Antarctic Intermediate water flow during the last deglaciation. Geochem. Geophys.
877 Geosys., 6(5). https://doi.org/10.1029/2004GC000858

878 Romanek, C.S., Grossman, E.L., Morse, J.W., (1992). Carbon isotopic fractionation in syn-
879 thetic aragonite and calcite: effects of temperature and precipitation rate. Geochimica et cos-
880 mochimica acta, 56(1), 419-430. https://doi.org/10.1016/0016-7037(92)90142-6

881 Santos, T.P., Ballalai, J.M., Franco, D.R., Oliveira, R.R., Lessa, D.O., Venancio, I.M., Chiessi,
882 C.M., Kuhnert, H., Johnstone, H., Albuquerque, A.L.S. (2020). Asymmetric response of the
883 subtropical western South Atlantic thermocline to the Dansgaard-Oeschger events of Marine
884 Isotope Stages 5 and 3. Quat. Sci. Rev., 236. https://doi.org/10.1016/j.quascirev.2020.106307

885 Santos, T.P., Lessa, D.O., Venancio, I.M., Chiessi, C.M., Mulitza, S., Kuhnert, H., Govin, A.,
886 Machado, T., Costa, K.B., Toledo, F., Dias, B.B., Albuquerque, A.L.S. (2017). Prolonged
887 warming of the Brazil Current precedes deglaciations. Earth Planet. Sci. Lett., 463, 1-12.
888 https://doi.org/10.1016/j.epsl.2017.01.014.

889 Schaefer, J.M., Putnam, A.E., Denton, G.H., Kaplan, M.R., Birkel, S., Doughty, A.M., Kelley,
890 S., Barrell, D.J.A., Finkel, R.C., Winckler, G., Anderson, R.F., Ninneman, U.S., Barker, S.,
891 Schwartz, R., Andersen, B.G., Schluechter, C., (2015). The Southern Glacial Maximum 65,000
892 years ago and its Unfinished Termination. Quat. Sci. Rev., 114, 52–60.
893 https://doi.org/10.1016/j.quascirev.2015.02.009

894 Schlitzer, R. (2017). Ocean Data View, odv.awi.de;

895 Schmitt, J., Schmitt, J., Schneider, R., Elsig, J., Leuenberger, D., Lourantou, A., Chappellaz,
896 J., Köhler, P., Joos, F., Stocker, T.F., Leuenberger, M., Fischer, H., (2012). Carbon isotope
897 constraints on the deglacial CO^2 rise from ice cores. Science, 336(6082), 711-714.
898 https://doi.org/10.1126/science.1217161

899 Schmittner, A., Lund, D.C., (2015). Early deglacial Atlantic overturning decline and its role in
900 atmospheric CO^2 rise inferred from carbon isotopes ($\delta^{13}C$). Clim. Past 11, 135–152.
901 https://doi.org/10.5194/cp-11-135-2015

902 Schneider, R., Schmitt, J., Köhler, P., Joos, F., Fischer, H., (2013). A reconstruction of atmos-
903 pheric carbon dioxide and its stable carbon isotopic composition from the penultimate glacial
904 maximum to the last glacial inception, Clim. Past, 9(6), 2507–2523,
905 doi:10.5194/cp-9-2507-2013.

906 Shao, J., Stott, L., Menviel, L., Ridgwell, A., Ödalen, M., Mohtadi, M., (2021). The Atmospheric
907 Bridge Communicated the $\delta^{13}C$ Decline during the Last Deglaciation to the Global Upper
908 Ocean. Clim. Past Discuss. 1–28. https://doi.org/10.5194/cp-2020-95

909 Skinner, L.C., Fallon, S., Waelbroeck, C., Michel, E., Barker, S., (2010). Ventilation of the
910 Deep Southern and Deglacial CO_2 Rise. Science 328, 1147–1151. https://doi.org/10.1126/sci-
911 ence.1183627

912 Sortor, R.N., Lund, D.C., (2011). No evidence for a deglacial intermediate water $\Delta^{14}C$ anomaly
913 in the SW Atlantic. Earth Planet. Sci. Lett. 310, 65–72.
914 https://doi.org/10.1016/j.epsl.2011.07.017

915 Spero, H.J., Bijma, J., Lea, D.W., Bernis, B.E., (1997). Effect of seawater carbonate concen-
916 tration on foraminiferal carbon and oxygen isotopes. Nature 390, 497–500.
917 https://doi.org/10.1038/37333

918 Spero, H.J., Deniro, M., (1987). The Influence of Symbiont Photosynthesis on the $\delta^{18}O$ and
919 $\delta^{13}C$ Values of Planktonic Foraminiferal Shell Calcite, Symbiosis, 4, 213–228.

920 Spero, H.J., Lea, D.W., (2002). The Cause of Carbon Isotope Minimum Events on Glacial
921 Terminations, Science, 296, 522–525. https://doi.org/10.1126/science.1069401

922 Sprintall, J., Tomczak, M., (1993). On the formation of Central Water and thermocline ventila-
923 tion in the southern hemisphere. Deep. Res. I. 40, 827-848. https://doi.org/10.1016/0967-
924 0637(93)90074-D;

925 Steph, S., Regenberg, M., Tiedemann, R., Mulitza, S., Nürnberg, D. (2009). Stable isotopes
926 of planktonic foraminifera from tropical Atlantic/Caribbean core-tops: Implications for recon-
927 structing upper ocean stratification. Mar. Micropaleontol., *71*(1–2), 1–19.
928 https://doi.org/10.1016/j.marmicro.2008.12.004;

929 Stramma, L., England, M. (1999). On the water masses and mean circulation of the South
930 Atlantic Ocean. J. Geophys. Res., v. 104, p. 20.863-20.883.
931 https://doi.org/10.1029/1999JC900139;

932 Talley, L.D., (1996). Antarctic Intermediate Water in the South Atlantic. In *The South Atlantic:*
933 *present and past circulation* (Ed. Wefer, G., Berger, W.H., Siedler, G., Webb, D.J.,) 219–238.
934 https://doi.org/10.1007/978-3-642-80353-6_11

935 Talley, L.D., (2013). Closure of the Global Overturning Circulation Through the Indian, Pacific,
936 and Southern Oceans: Schematics and Transports. Oceanography 26, 80–97.
937 https://doi.org/10.5670/oceanog.2013.07

938 Tapia, R., Nürnberg, D., Ho, S.L., Lamy, F., Ullermann, J., Gersonde, R., Tiedemann, R.,
939 (2019). Glacial differences of Southern Ocean Intermediate Waters in the Central South Pa-
940 cific. Quat. Sci. Rev. 208, 105–117. https://doi.org/10.1016/j.quascirev.2019.01.016

941 Tessin, A.C., Lund, D.C., (2013). Isotopically depleted carbon in the mid-depth South Atlantic
942 during the last deglaciation. Paleoceanography 28, 296–306.
943 https://doi.org/10.1002/palo.20026

Toggweiler, J.R., Russell, J.L., Carson, S.R., (2006). Midlatitude westerlies, atmospheric CO_2, and climate change during the ice ages, Paleoceanography 21, 1–15. https://doi.org/10.1029/2005PA001154

Toggweiler, J.R., Samuels, B., (1995). Effect of Drake Passage on the global thermohaline. Deep. Res. I 42, 477–500. https://doi.org/10.1016/0967-0637(95)00012-U

Tomczak, M., Godfrey, J.S., (1994). Regional Oceanography, 1st ed, Regional Oceanography. Elsevier.

Ujiié, Y., de Garidel-Thoron, T., Wantanabe, S., Wiebe, P., de Vargas, C. (2010). Coiling dimorphism within a genetic type of the planktonic foraminifer *Globorotalia truncatulinoides*. Mar. Micropaleontol., 77(3-4), 145–153. https://doi.org/10.1016/j.marmicro.2010.09.001

Venancio, I.M., Mulitza, S., Govin, A., Santos, T.P., Lessa, D.O., Albuquerque, A.L.S., Chiessi, C.M., Tiedemann, R., Vahlenkamp, M., Bickert, T., Schulz, M., (2018). Millennial- to orbital-scale responses of Western Equatorial Atlantic thermocline depth to changes in the trade wind system since the last interglacial. Paleoceanogr. Paleoclimatol., *33*(12), 1490–1507. https://doi.org/10.1029/2018PA003437;

Voigt, I., Cruz, A.P.S., Mulitza, S., Chiessi, C.M., Mackensen, A., Lippold, J., Antz, B., Zabel, M., Zhang, Y., Barbosa, C.F., Tisserand, A.A., (2017). Variability in mid-depth ventilation of the western Atlantic Ocean during the last deglaciation. Paleoceanography 32, 948–965. https://doi.org/10.1002/2017PA003095

WAIS (West Antarctic Ice Sheet Project) members (2013). Onset of deglacial warming in West Antarctica driven by local orbital forcing. Nature 500, 440–444. https://doi.org/10.1038/nature12376

Wilke, I., Bickert, T., Peeters, F.J.C., (2006). The influence of seawater carbonate ion concentration [CO_3^{2-}] on the stable carbon isotope composition of the planktic foraminifera species

968 *Globorotalia inflata*. Mar. Micropaleontol. 58, 243–258. https://doi.org/10.1016/j.marmi-
969 cro.2005.11.005

970 Wolff, E.W., Chappellaz, J., Blunier, T., Rasmussen, S.O., Svensson, A., (2010). Millennial-
971 scale variability during the last glacial: The ice core record. Quat. Sci. Rev., 29(21-22), 2828-
972 2838. https://doi.org/10.1016/j.quascirev.2009.10.013

973 Wolff, E.W., Fischer, H., Röthlisberger, R., (2009). Glacial terminations as southern warmings
974 without northern control. Nat. Geosci. 2, 206–209. https://doi.org/10.1038/ngeo442

975 Zhang, J., Quay, P.D., Wilbur, D.O., 1995. Carbon-isotope fractionation during gaswater ex-
976 change and dissolution of CO_2. Geochim. Cosmochim. Acta 59, 107–114.
977 https://doi.org/10.1016/0016-7037(95)91550-D

978 Zhang, Y., Chiessi, C.M., Mulitza, S., Sawakuchi, A.O., Häggi, C., Zabel, M., Portilho-Ramos,
979 R.C., Schefuß, E., Crivellari, S., Wefer, G., (2017). Different precipitation patterns across trop-
980 ical South America during Heinrich and Dansgaard-Oeschger stadials. Quat. Sci. Rev., *177*,
981 1-9. https://doi.org/10.1016/j.quascirev.2017.10.012

982 Ziegler, M., Diz, P., Hall, I.R., Zahn, R., (2013). Millennial-scale changes in atmospheric CO_2
983 levels linked to the Southern Ocean carbon isotope gradient and dust flux. Nat. Geosci. 6,
984 457–461. https://doi.org/10.1038/ngeo1782

985 Zweng, M. M., J. R. Reagan, D. Seidov, T. P. Boyer, R. A. Locarnini, H. E. Garcia, A. V.
986 Mishonov, O. K. Baranova, K. Weathers, C. R. Paver, and I. Smolyar, 2018. World Ocean
987 Atlas 2018, Volume 2: Salinity. A. Mishonov Technical Ed.; NOAA Atlas NESDIS 82, 50pp.

988

989